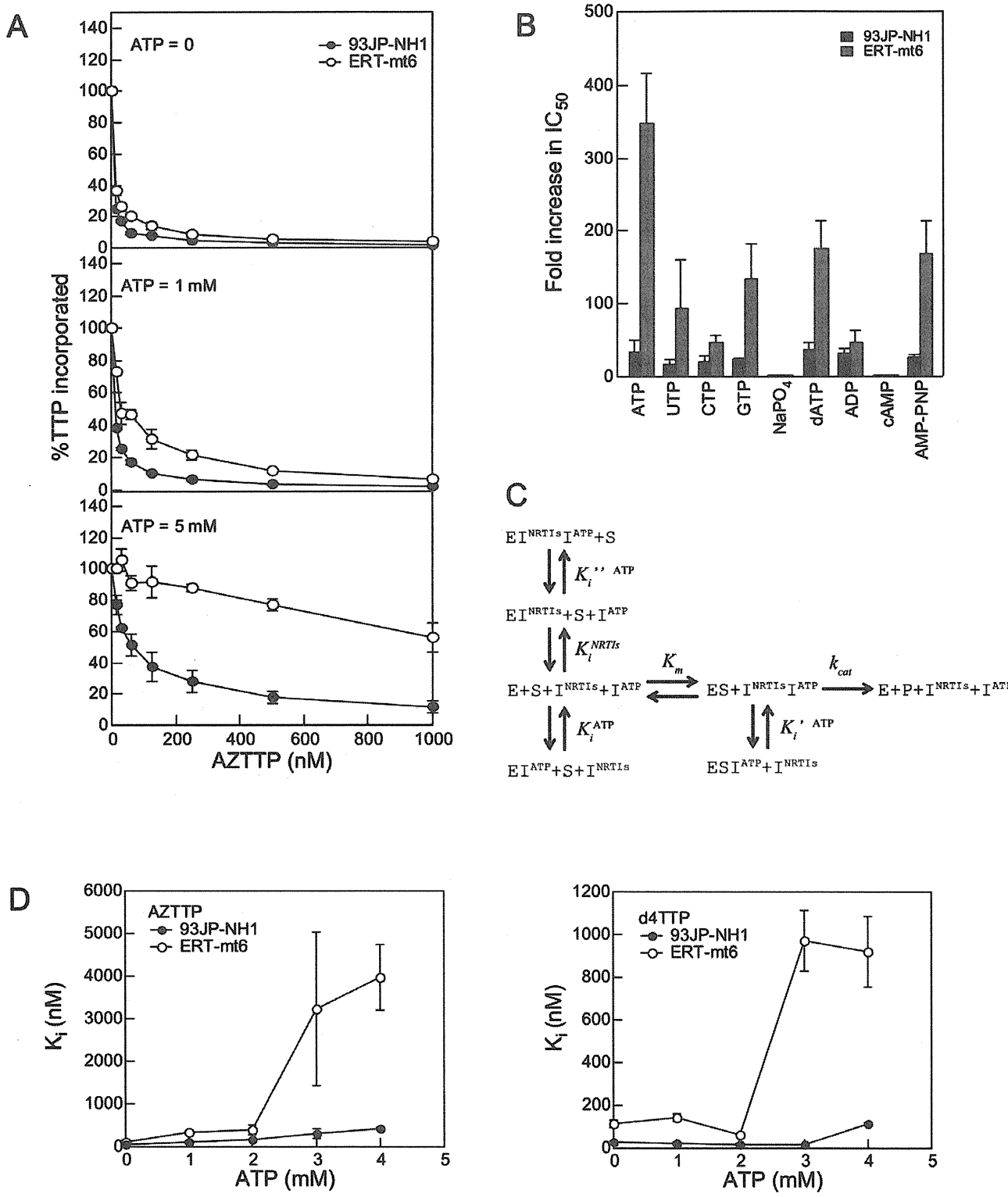

Figure 2. Effects of ATP on NRTI action. A. Effects of ATP on AZTTP-dependent inhibition of RT activities. The dTMP incorporation into poly (rA)·p(dT)$_{12-18}$ was measured using [α-^{32}P]dTTP and purified p51/p66 heterodimers in the presence of the indicated concentrations of ATP and AZTTP. Ratios of the dTTP incorporation at given concentrations of AZTTP to that in the absence of AZTTP are shown. **B.** Effects of nucleotides and related compounds on IC$_{50}$s of AZTTP. IC$_{50}$s of AZTTP were determined in the presence of 5 mM of the indicated compounds, and the fold increases in IC$_{50}$ compared to AZTTP without the compounds are shown. **C.** A simplified kinetics model of DNA polymerization in the presence of ATP and NRTI. The model was generated on the basis of the kinetics data in Figure 1 and Figure S2, previously reported kinetics data [17,18], and a crystal structure study of the ATP-RT complex [11]. **D.** Effects of ATP on the K_i values of AZTTP and d4TTP. The K_i^{AZTTP} and K_i^{d4TTP} values were estimated by fitting the initial velocity of dTTP incorporation to Equation 5 as described in Materials and Methods. The mean values with variances are shown for two independent experiments performed with duplicate samples.

doi:10.1371/journal.pone.0008867.g002

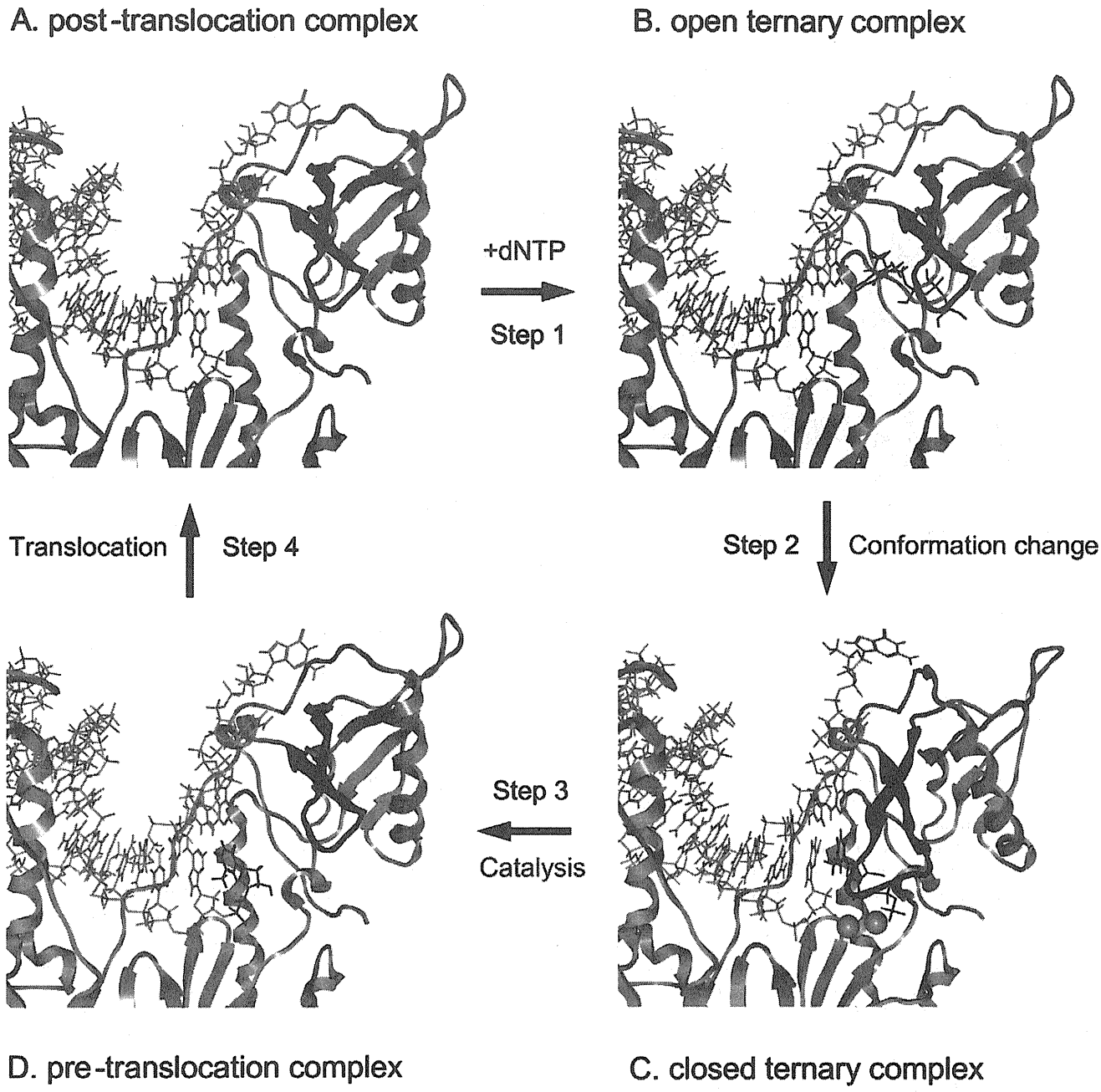

Figure 3. Structural models of the HIV-1 RT p66 subunit in a DNA polymerization cycle. The 3-D models of the 93JP-NH1 p66-template-primer ternary complex of the fingers-open configuration at post-translocation (**A**), fingers-open configuration at the stage of dTTP binding (**B**), fingers-closed configuration after fingers-rotation (**C**), and fingers-open configuration at pre-translocation stage (**D**). The models were constructed by homology modeling and docking simulation techniques using two crystal structures [1,14] of the HIV-1 RTs as modeling templates (see Materials and Methods). Catalytic clefts composed of fingers, palm, and thumb subdomains are shown. dTTP, magenta sticks; p66 main chain, grey ribbon; Mg^{2+} ion, gray spheres; template-primer, grey sticks; β3-β4 loop of the fingers subdomain, blue ribbon.
doi:10.1371/journal.pone.0008867.g003

along the highly conserved motif A near the side chains of R72, D110, D113, F116, D185, and K219 residues at the p66 fingers subdomain of both RTs (Figure 4). The ATP-binding position was stabilized through electrostatic and hydrophobic interactions between the ATP molecule and the side chains of surrounding amino acids. The ATP position was similar to the ATP position in the crystal structure of the template-primer-free RT [11] and was indistinguishable between the pre- and post-translocation stages (Figure S3), suggesting that a specific ATP-binding site is preserved in the free-RT and RT-template-primer tertiary complex. The ATP-binding position was distinct from that of dNTP at initial binding [23] and after fingers-domain rotation [1] in the fingers-open and -closed configurations of RT, respectively (Figures 3 and 4), consistent with our kinetic data for allosteric regulation (Figures 1 and 2).

The bound ATP molecule was located near the YMDD motif, motif A, and the 3′-end of the primer, suggesting that the ATP binding can modulate polymerization and support the excision

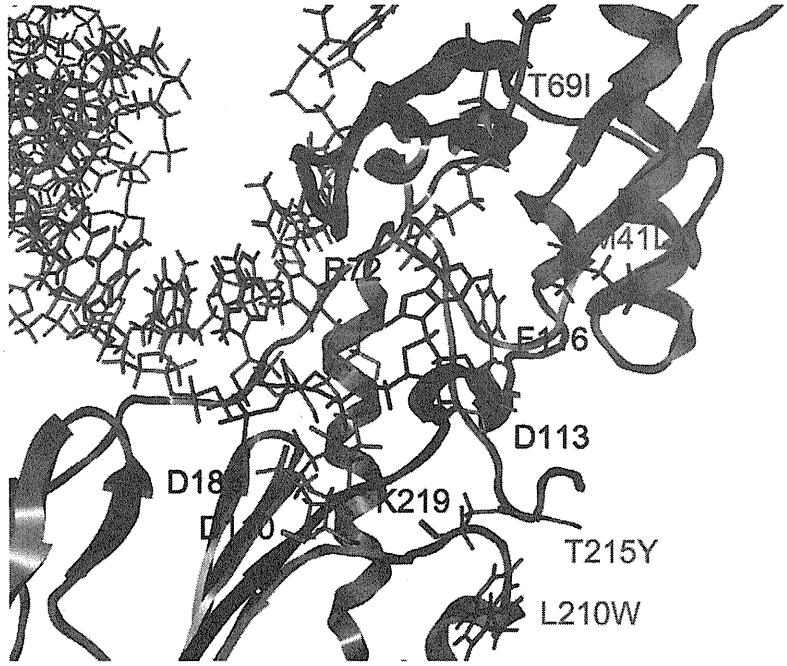

Figure 4. Docking simulations of ATP to the HIV-1 RT p66 subunit with NRTI resistance. ATP was docked with the optimized p66-template-primer complex of the ERT-mt6 strain at the pre-translation stage, using the automated ligand docking program ASEDock2005 [22] operated in the Molecular Operating Environment (see Materials and Methods). Catalytic clefts composed of fingers, palm, and thumb subdomains are shown. ATP, red sticks; p66 main chain, grey ribbon; template-primer, grey sticks; motif A, blue ribbon. The side chains of amino acids around ATP are indicated with cyan sticks, and the side chains of amino acids for NRTI resistance (M41L, T69I, L210W, and T215W) with orange sticks. The main chain of an 11-amino-acid insertion at the β3-β4 loops for NRTI resistance is shown in orange.
doi:10.1371/journal.pone.0008867.g004

reaction (Figure 4). The bound ATP molecule was positioned between the catalytic site and the β3-β4 loops, suggesting that the ATP binding can modulate the initial binding and translocation of dNTP and NRTIs into the catalytic site (Figures 3 and 4). Taken together, these structural data are well consistent with our kinetic data, biochemical data for excision [8,9,10], and crystal structure data for ATP binding [11].

NRTI-resistance mutations of the ERT-mt6 p66 (Figure 4, orange residues) were located relatively far away from the bound ATP molecule and catalytic center in p66. Thus, it is less likely that these mutations directly influence the ATP-mediated excision. Instead, the M41L, T69I, L210W, and T215Y substitutions augmented the hydrophobicity of the catalytic cavity of p66, which could enhance p66's ability to exclude water from the catalytic site cleft for a higher fidelity of nucleotide selection [6,29]. This possibility is consistent with our kinetic data. The fingers-domain insertion induced changes in the shape of the β3-β4 loops that could alter the position of the initial binding site of dNTP and NRTI relative to the catalytic site.

Site-Directed Mutagenesis Study

We further examined how substitutions of amino acids around the predicted ATP-binding site would influence the biochemical properties of the ERT-mt6 RT. Single-amino-acid substitutions were introduced into the p66 chain of ERT-mt6, and their effects on the overall DNA polymerization activity, IC_{50} of AZTTP, K_m value, k_{cat} value, and K_i value of ATP for the ERT-mt6 RT were analyzed. The positions of the substitutions introduced corresponded to positions 72, 110, 113, 116, and 219 of the 93JP-NH1 p66. We did not conduct mutagenesis of D185 in the YMDD loops, because its essential role in the translocation of the template primer has been established [14]. All of the tested substitutions changed the overall DNA polymerization activity of the RT (Figure S4B). The substitutions at positions 72, 110, and 116 (R72A/Q, D110A/N, and F116A/L) resulted in a loss of DNA polymerization activity, suggesting their essential role in this activity. In contrast, those at positions 113 and 219 (D113A/N and K219Q/A) enhanced the incorporation of dTTP (Figure S4B), suggesting their regulatory role in overall DNA polymerization activity.

The active D113A/N and K219Q/A RTs were further examined for changes in the IC_{50} of AZTTP, and in the K_m, k_{cat}, K_i^{ATP}, and $K_i'^{ATP}$ values. The D113A/N resulted in an approximately 4- to 5-fold reduction in the IC_{50} of AZTTP (Figure S4C), suggesting that D113 plays an important role in the development of NRTI resistance. K_m, k_{cat}, K_i^{ATP}, and $K_i'^{ATP}$ values were estimated by using the substrate-velocity curves for the D113A/N and K219Q/A RTs (Figure S4D). The D113A/N and K219Q/A substitutions induced changes in the K_m, k_{cat}, K_i^{ATP}, and $K_i'^{ATP}$ values, suggesting that the D113 and K219 residues regulate the K_m of substrate, k_{cat}, and K_i values of ATP (Figure 5). The D113A/N substitutions resulted in reductions in K_m and k_{cat} values, which paralleled the reductions in K_i^{ATP} and $K_i'^{ATP}$ values. The K219Q/A substitutions resulted in increases in K_m values, which paralleled the increases in K_i^{ATP} values. The kinetics data implied that residues 113 and 219 can regulate the affinity of the substrate and ATP molecule but do not contribute directly to the catalysis of DNA polymerization, suggesting that the ATP binding site would be distinct from the catalytic site for DNA polymerization.

Discussion

How HIV-1 RT regulates the nucleotide selectivity for DNA synthesis is a central issue for genetics and the NRTI resistance of

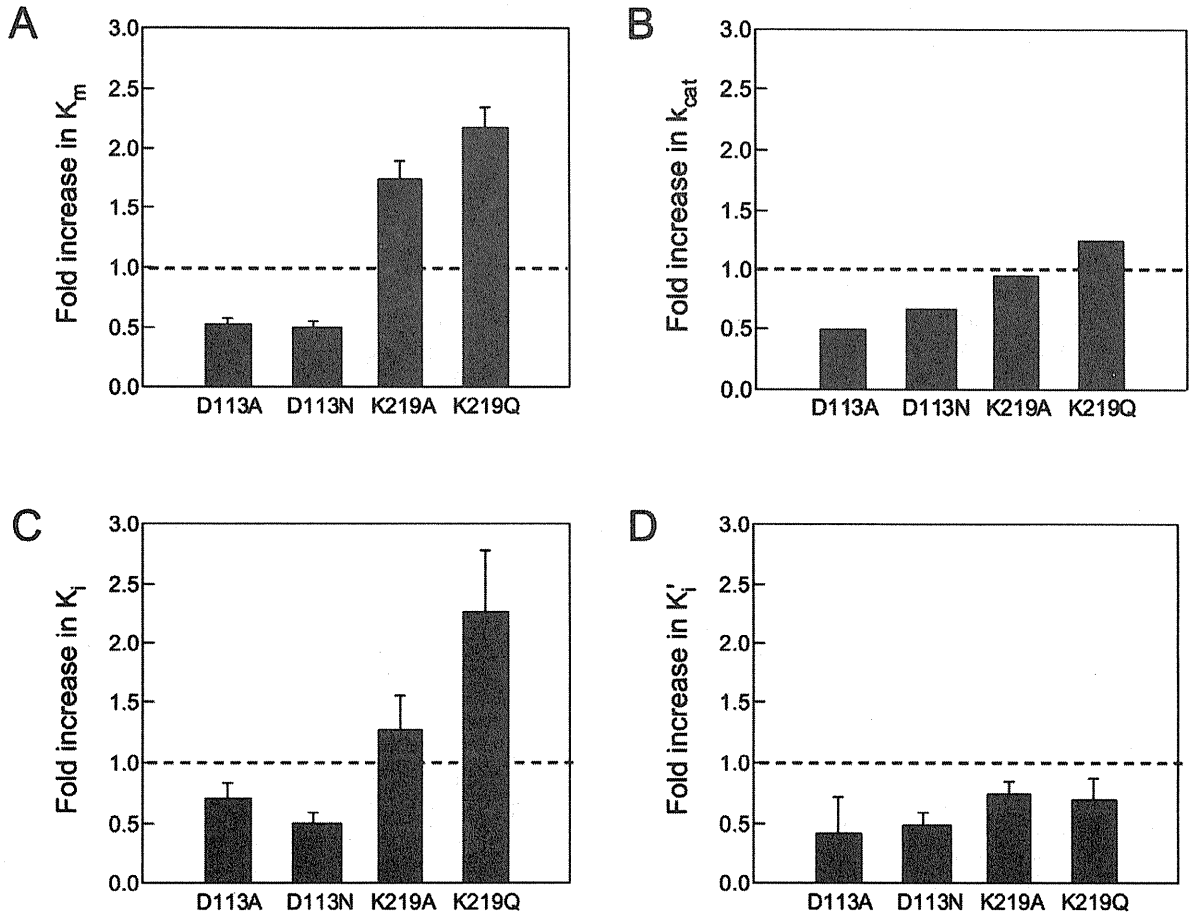

Figure 5. Site-directed mutagenesis study of the HIV-1 RT p66 subunit with NRTI resistance. Single substitutions of amino acids around the predicted ATP-binding site in Figure 3 were introduced into the p66 chain of ERT-mt6. The overall DNA polymerization activity (Figure S4B), IC_{50} of AZTTP (Figure S4C), and K_m, k_{cat}, K_i^{ATP}, and $K_i'^{ATP}$ values were measured using the [α-^{32}P]dTTP and poly (rA)·p(dT)$_{12-18}$ system, and fold increases in the K_m (**A**), k_{cat} (**B**), K_i^{ATP} (**C**), and $K_i'^{ATP}$ values (**D**) compared to those for the ERT-mt6 were calculated. Results for the RT mutants, D113A, D113N, K219Q, and K219A, which retained sufficient polymerization activity for a kinetic study, are shown.
doi:10.1371/journal.pone.0008867.g005

HIV-1. In this study, we showed that the ATP molecule at physiological concentrations acted as an allosteric regulator of HIV-1 RT to modulate nucleotide selectivity. We also showed probable 3-D positions of the bound ATP molecule and NRTI mutations in the catalytic cleft; these positions immediately suggested that a nucleotide-selection mechanism—i.e., an ATP- and RT-mutation-mediated modulation of the geometric selection of nucleotides—played a role in the DNA polymerization and NRTI resistance of HIV-1.

First, we demonstrated that the ATP molecule modulated the K_m and k_{cat} values of the substrate for HIV-1 RT. We showed that the ATP molecule reduced the K_m values of dTTP with both NRTI-sensitive and -resistant RTs (Figure 1C). These results suggested that the ATP molecule can decrease the K_m value of a natural substrate to HIV-1 RT. We also showed that the ATP molecule reduced the k_{cat} values of these RTs (Figure 1C). These results suggested that the ATP molecule can decrease the rate of DNA polymerization and thereby increase the probability of an excision reaction by HIV-1 RT. Lineweaver-Burk double-reciprocal plots showed that the ATP molecule is a mixed noncompetitive inhibitor of RT, suggesting distinct binding sites for ATP and dNTP. Taken together, these data strongly suggest that the ATP molecule can act as an allosteric regulator to modulate the nucleotide selectivity of HIV-1 RT.

We next investigated the mechanisms by which the ATP molecule modulates the nucleotide selectivity of HIV-1 RT. Docking simulations predicted that the ATP-binding site would be similar between NRTI-sensitive and -resistant RTs during DNA polymerization. Consistent with the results of the kinetic study, the predicted ATP-binding site was distinct from that of dNTP and NRTIs [23], and single-amino-acid substitutions at positions 113 and 219 around the predicted ATP-binding site indeed induced significant changes in the K_i value of ATP. Importantly, the ATP-binding position suggested possible mechanisms by which ATP could influence DNA polymerization and the excision reactions of RT, as follows: First, interactions between the γ-phosphate of the ATP molecule and the side chain of D185 in the YMDD loops could influence the DNA translocation of the primer template [14]. Second, interactions between charged portions of the ATP molecule and the side chains of D110 and D185 could modulate the Mg^{2+} position and stability for DNA polymerization [1]. Third, the γ-phosphate of the ATP molecule is located near the 5′ phosphate of DNA primer terminus and thus could increase the probability of a DNA excision [11] in concert with a reduction in the k_{cat} value of RT.

We found no marked increases in the K_i values of AZTTP and d4TTP at the ATP concentrations around the $K_i'^{ATP}$ value (1.1±0.4 mM) for ATP binding to the RT-template-primer-dTTP

complex for the excision reaction (Figures 2C and 2D). The ATP molecule was estimated to bind with equivalent K_i values to the NRTI-sensitive and -resistant RTs, as others have indicated [15,16], suggesting that NRTI-resistance mutations do not necessarily increase ATP-binding affinity. Moreover, some NRTI-resistant mutations, such as M41L and T69I, are located relatively distantly from the ATP-binding site and catalytic site (Figure 4), which makes their direct impact on DNA excision unlikely. Thus, our study suggests that an ATP-mediated DNA excision mechanism alone is insufficient to explain the roles of the NRTI-resistance mutations, as was also noted previously [12]. Therefore, we speculate that NRTI-resistance mutations can decrease the affinity of NRTIs to HIV-1 RT in concert with the ATP molecule.

Our data imply that the ATP molecule and NRTI mutations can modulate the nucleotide selectivity of HIV-1 RT by influencing the geometric selection of nucleotides in the catalytic cavity, as follows: First, the presence of bound ATP molecule in the catalytic cavity can sterically influence the initial binding and translocation of dNTP/NRTI into the catalytic site. Second, more hydrophobic side chains of the NRTI-resistance mutations can improve p66's ability to exclude water from the catalytic cavity and allow more intimate interactions between nucleotides, the primer-template, and amino acids around the catalytic site for distinguishing between correct and incorrect base pairs. In this regard, previous crystal structure analyses have revealed that the active site of a low-fidelity polymerase is more accessible to the solvent than those of more accurate polymerases [30,31]. Third, K_i^{NRTIs} values increased sharply with NRTI-resistant RT (ERT-mt6 RT) at ATP concentrations around the K_i^{ATP} value (2.8±1.3 mM) for ATP binding to the RT-template-primer complex (Figures 2C and 2D). Fourth, the changes in the K_m value of dTTP correlated with those in the K_i value of the ATP molecule to the RT-template-primer complex (Figures 5A and 5C). Taken together, our structural, kinetic and mutagenesis data suggest that the NRTI-resistance mutations and the ATP molecule can cooperatively modulate physicochemical properties of the p66 catalytic cavity to alter the fidelity of the geometric selection of nucleotides and the probability of an excision reaction.

In conclusion, we demonstrated that the ATP molecule at physiological concentrations acts as an allosteric regulator of HIV-1 RT to decrease the K_m value of the substrate, decrease the k_{ca} value$_b$ and increase the K_i value of NRTIs for RT. The effects were independent of NRTI-resistance mutations of RT. The ATP molecule and NRTI mutations could decrease RT's sensitivity to NRTI of RT in concert with the RT mutation. Our data support the notion that the ATP molecule and NRTI mutations can modulate nucleotide selectivity by altering the fidelity of the geometric selection of nucleotides and the probability of an excision reaction.

Materials and Methods

Nucleotides

Poly(rA)•p(dT)$_{12-18}$, dNTPs (100 mM, pH 7.5), NTPs (100 mM, pH 7.5), and [α-^{32}P]dTTP were purchased from Pharmacia Biotech Inc. (USA). ADP and AMP were from ICN (USA). Adenosine 5′-(β, γ-imido) triphosphate (AMP-PNP) was from Sigma Chemical (USA). 3′-Azido 3′-deoxythymidine 5′-triphosphate (AZTTP), 3′-deoxy-2′, and 3′-didehydrothymidine 5′-triphosphate (d4TTP) were from Moravek Biochemicals (USA).

Expression and Purification of HIV-1 RT

HIV-1 infectious molecular clones, 93JP-NH1 and ERT-mt6 [13], were used to clone and express the p51 and p66 subunits of the HIV-1 RT. The open reading frames encoding the RT p51 and p66 subunits of the 93JP-NH1 and ERT-mt6 RTs were amplified by PCR and cloned into the BamH1 site of pQE-9 (Qiagen, Germany). The nucleotide sequences of the PCR-amplified fragments and the sequences around the cloning sites were verified with an automated sequencer. Each subunit was expressed individually in XL1-blue by induction with isopropyl-β-D-thiogalactopyranoside, and the cells expressing p51 and p66 were mixed in binding buffer (20 mM sodium phosphate, 500 mM NaCl, 10 mM imidazole, and EDTA-free protease inhibitor mixture (Roche, Germany), lysed with a French press, centrifuged at 10,000 g for 20 min, and filtered (0.45-μm pore size). The p51/p66 heterodimers were purified from the filtered lysates by Ni^{2+} affinity chromatography (HiTrap Chelating HP; Amersham Biosciences, UK) and size exclusion chromatography (HiLoad 16/60 Superdex 200 pg; Amersham Biosciences, UK). All of the purification processes were carried out at 4°C. About 1.5 (ERT-mt6) and 3 mg (93JP-NH1) of the p51/p66 heterodimers with greater than 95% purity as judged by SDS-polyacrylamide gel electrophoresis (Figure S1) were obtained with a 1-liter culture. The specific activities of the purified RTs were 40,000 and 10,000 units/mg of protein for 93JP-NH1 and ERT-mt6, respectively, wherein one unit is defined as the amount of enzyme required for incorporation of 1.0 nmol of ^{32}P-dTTP into poly(rA)/poly(dT)$_{12-18}$ in 10 min at 37°C.

Measurement of RT Activity

The purified RTs were dissolved in the RT stock buffer (50 mM Tris-HCl pH 7.5, 75 mM KCl, 5 mM $MgCl_2$, 2 mM DTT, 0.05% NP40, and 50% glycerol)[32,33] and kept at −30°C until use. RNA-dependent DNA polymerase activity was measured using [α-^{32}P]dTTP and poly(rA)/poly(dT)$_{12-18}$ as described previously [33]. For the RT reaction in the presence of ATP, RT activities were measured in 100 μl of RT reaction cocktail consisting of 50 mM Tris-HCl pH 7.5, 75 mM KCl, 5 mM $MgCl_2$, 2 mM DTT, 0.05% NP40, and 50% glycerol containing RT (1–10 nM), dTTP (0.2–18 μM), and ATP (0–4 mM). For the RT reaction in the presence of ATP and NRTI, RT activities were measured in 100 μl of the RT reaction cocktail containing RT (1–10 nM), dTTP (0.2–18 μM), ATP (0–5 mM), and AZTTP or d4TTP (0–1 μM). These experiments were performed in duplicate and repeated two to six times.

Steady-State Kinetic Analysis

The averages of the experimental data were fit by a nonlinear regression method using the program Igor Pro (WaveMetrics, USA). The kinetics parameters were determined by the Michaelis-Menten equation:

$$v = \frac{V_{\max}{}^{app}[S]}{K_m{}^{app} + [S]}, \quad (1)$$

where $[S]$ is the substrate concentration; $K_m{}^{app}$ is the apparent Michaelis-Menten constant; and $V_{max}{}^{app}$ is the apparent maximal rate attained when the enzyme active sites are saturated by substrate.

Based on the kinetics data in Figure 1 and Figure S2, the previously reported kinetics data [17,18], and a crystal structure study of the ATP-RT complex [11], we assumed mixed noncompetitive inhibition of ATP and competitive inhibition of NRTIs (Figure 2C).

Using this model, the enzyme kinetic parameters were calculated using Equations 2–5.

$V_{max}{}^{app}$ and $K_m{}^{app}$ are defined as

$$V_{\max}{}^{app} = k_{cat}{}^{app}[E] \quad (2)$$

and

$$K_m{}^{app} = K_m \frac{(1+\frac{[I]}{K_i})}{(1+\frac{[I]}{K_i'})}, \quad (3)$$

respectively, where K_m is the Michaelis-Menten constant; $[E]$ is the enzyme concentration; $[I]$ is the inhibitor concentration; K_i and K_i' are the inhibition constants for the enzyme and the complex of the enzyme with substrate; and $k_{cat}{}^{app}$ is the apparent turnover number:

$$k_{cat}{}^{app} = \frac{k_{cat}}{(1+\frac{[I]}{K_i'})}, \quad (4)$$

where k_{cat} is the turnover number.

The $k_{cat}{}^{app}$ and $K_m{}^{app}$ that can be derived from the model (Figure 2C) are

$$k_{cat}{}^{app} = \frac{k_{cat}}{(1+\frac{[I^{ATP}]}{K_i'^{ATP}})} \quad (5)$$

and

$$K_m{}^{app} = \frac{K_m(1+\frac{[I^{ATP}]}{K_i^{ATP}}+\frac{[I^{AZT}]}{K_i^{AZT}}+\frac{[I^{AZT}][I^{ATP}]}{K_i''^{ATP}K_i^{AZT}})}{(1+\frac{[I^{ATP}]}{K_i'^{ATP}})}, \quad (6)$$

where K_i^{ATP} is the dissociation constant of ATP; K_i^{AZTTP} is the dissociation constant of AZTTP; $[I^{ATP}]$ is the ATP concentration; and $[I^{AZTTP}]$ is the AZTTP concentration.

Structural Analysis

We constructed the 3-D models of HIV-1 RTs by homology modeling [19] using the Molecular Operating Environment, MOE (Chemical Computing Group, Canada) as previously described [34]. We generated models of the 93JPNH-1 RT and ERT-mt6 RT structures at the pre- and post-translocation stages, which theoretically are competent for the binding of the incoming-ATP. We used two crystal structures of the HIV-1 RTs (PDB code: 1N6Q [14] and 1RTD [1]) as modeling templates. The sequence identities of the 1N6Q and 1RTD with the 93JPNH-1 RT and ERT-mt6 RT are ~90%. We optimized the 3-D structure thermodynamically by energy minimization using MOE and an AMBER94 force field. We further refined the physically unacceptable local structure of the models on the basis of evaluation by the Ramachandran plot using MOE. The optimized models were docked with ATP with the automated ligand docking program ASEDock2005 [22] (Ryoka Systems, Japan) operated in the Molecular Operating Environment. The RT-template-primer-ATP complex structures were thermodynamically and sterically optimized as described above.

Site-Directed Mutagenesis

Site-directed mutagenesis was performed with a QuikChange Multi Site-Directed Mutagenesis Kit (Stratagene, USA), using pQE70 (Qiagen, Germany) containing the coding sequence of the p66 subunit of ERT-mt6 as the template. The positions of the amino acid substitutions corresponded to the positions 72, 110, 113, 116, and 219 of 93JP-NH1. The mutations and oligonucleotides used in the mutagenesis reaction were R72A (5′-CGGCCAGCA TTAAATGGgcGAAATTAGTAGATTTCAGAGAG-3′), R72Q (5′-CGGCCAGCATTAAATGGcaGAAATTAGTAGATTTCA-GAGAG-3′), D110A (5′-GAAAAAATCAGTAACAGTACTAG-cTGTGGGAGATGCATATTTTTC-3′), D110N (5′-GAAAAA-ATCAGTAACAGTACTAaATGTGGGAGATGCATATTTT-TC-3′), D113A (5′-CAGTACTAGATGTGGGAGcTGCATAT-TTTTCAGTTCCTT-3′), D113N (5′-CAGTACTAGATGTGG-GAaaTGCATATTTTTCAGTTCCTT-3′), F116A (5′-GGAA-CTGAAgcATATGCATCTCCCACATCTAGTACTG-3′), F116L (5′-GGAACTGAcAAATATGCATCTCCCACATCTAGTACT-G-3′), K219A (5′-GGGATTTTATACACCAGACgcAAAGCAT-CAGAAGGAACCTC-3′), and K230(219)Q (5′-GGGATTTTA-TACACCAGACcAAAAGCATCAGAAGGAACCTC-3′), where the introduced mutations appear in lowercase letters. In all cases, the nucleotide sequences of the complete p66 coding region and of cloning sites were verified with an automated sequencer. The mutant p66 subunits were expressed in XL1-blue and used to form the p51/p66 heterodimer using the p51 subunit of 93JP-NH1 in binding buffer, as described above. The p51/p66 heterodimers were purified by Ni^{2+} affinity chromatography. About 104 to 221 μg of the p51/p66 heterodimers, with about 90% purity as judged by SDS-polyacrylamide gel electrophoresis (Figure S4A), were obtained from a 20 ml culture. The purified RTs were dissolved in the RT stock buffer and kept at −30°C until use.

Supporting Information

Figure S1 Data on RTs of 93JP-NH1 and ERT-mt6. A. Electrophoresis of the purified p51/p66 heterodimers of HIV-1 RTs. The purified p51/p66 heterodimers of 93JP-NH1 RT (NH1) and ERT-mt6 RT (mt6) were electrophoresed on an SDS-4/20% polyacrylamide gradient gel. The gel was stained with GelCode Blue Stain Reagent (Pierce, USA). (Lanes 1 and 4) Molecular size markers. B. The substrate-velocity curves of purified HIV-1 RTs. RNA-dependent DNA polymerase activity at the indicated concentrations of [α-^{32}P]dTTP was measured using purified RTs of 93JP-NH1 (1 nM) and ERT-mt6 (10 nM).
Found at: doi:10.1371/journal.pone.0008867.s001 (0.29 MB TIF)

Figure S2 Lineweaver-Burk double-reciprocal plots of AZTTP-dependent inhibition of dTTP incorporation. A. 93JP-NH1 RT. B. ERT-mt6. The initial velocities of dTMP incorporation into poly (rA)·p(dT)$_{12-18}$ were measured using [α-^{32}P]dTTP and purified RTs in the presence of AZTTP. Reciprocal values of the initial velocities and substrate concentrations are plotted.
Found at: doi:10.1371/journal.pone.0008867.s002 (0.15 MB TIF)

Figure S3 Docking simulations of ATP with RT-template-primer ternary complex models. A and C: 93JP-NH1 RT. B and D: ERT-mt6 RT. The 3-D models of the p66-template-primer complexes at the pre-translation stage (A and B) and the post-translation stage (C and D) were constructed by a homology modeling technique and docked with ATP using the ASEDock2005 (see Materials and Methods). Catalytic clefts composed of fingers, palm, and thumb subdomains are shown. ATP, red sticks; p66 main chain, grey ribbon; template-primer, grey sticks; motif A, blue ribbon.
Found at: doi:10.1371/journal.pone.0008867.s003 (1.93 MB TIF)

Figure S4 Data on RT mutants from the ERT-mt6 RT. A. Electrophoresis of the purified RT mutants from the ERT-mt6 RT. B. dTMP incorporations into poly (rA)·p(dT)$_{12-18}$ by the

mutant RTs. RNA-dependent DNA polymerase activity of the purified RTs (20 nM) was measured using a [α-^{32}P]dTTP and poly (rA)·p(dT)$_{12-18}$ system. C. Fold increases in the IC_{50} of AZTTP by ATP addition. IC_{50} values of AZTTP with RT mutants were calculated from the amounts of [α-^{32}P]dTTP incorporation in the presence of various concentrations (0–1 μM) of AZTTP and 5 mM ATP. Fold increases in IC_{50} compared to the values without ATP are shown. D. The substrate-velocity curves of purified HIV-1 RTs in the presence of ATP. RNA-dependent DNA polymerase activity of the purified mutant RTs was measured using various concentrations of [α-^{32}P]dTTP and poly (rA)·p(dT)$_{12-18}$ in the presence of ATP. Representative results with D113A RT (left) and K219A RT (right) are shown.
Found at: doi:10.1371/journal.pone.0008867.s004 (0.39 MB TIF)

Author Contributions

Conceived and designed the experiments: MY HS. Performed the experiments: MY HM. Analyzed the data: MY. Wrote the paper: MY HS.

References

1. Huang H, Chopra R, Verdine GL, Harrison SC (1998) Structure of a covalently trapped catalytic complex of HIV-1 reverse transcriptase: implications for drug resistance. Science 282: 1669–1675.
2. Preston BD, Poiesz BJ, Loeb LA (1988) Fidelity of HIV-1 reverse transcriptase. Science 242: 1168–1171.
3. Roberts JD, Bebenek K, Kunkel TA (1988) The accuracy of reverse transcriptase from HIV-1. Science 242: 1171–1173.
4. Goodman MF (1997) Hydrogen bonding revisited: geometric selection as a principal determinant of DNA replication fidelity. Proc Natl Acad Sci U S A 94: 10493–10495.
5. Kunkel TA, Bebenek K (2000) DNA replication fidelity. Annu Rev Biochem 69: 497–529.
6. Kunkel TA (2004) DNA replication fidelity. J Biol Chem 279: 16895–16898.
7. Traut TW (1994) Physiological concentrations of purines and pyrimidines. Mol Cell Biochem 140: 1–22.
8. Meyer PR, Matsuura SE, So AG, Scott WA (1998) Unblocking of chain-terminated primer by HIV-1 reverse transcriptase through a nucleotide-dependent mechanism. Proc Natl Acad Sci U S A 95: 13471–13476.
9. Arion D, Kaushik N, McCormick S, Borkow G, Parniak MA (1998) Phenotypic mechanism of HIV-1 resistance to 3′-azido-3′-deoxythymidine (AZT): increased polymerization processivity and enhanced sensitivity to pyrophosphate of the mutant viral reverse transcriptase. Biochemistry 37: 15908–15917.
10. Meyer PR, Matsuura SE, Mian AM, So AG, Scott WA (1999) A mechanism of AZT resistance: an increase in nucleotide-dependent primer unblocking by mutant HIV-1 reverse transcriptase. Mol Cell 4: 35–43.
11. Das K, Sarafianos SG, Clark AD Jr, Boyer PL, Hughes SH, et al. (2007) Crystal structures of clinically relevant Lys103Asn/Tyr181Cys double mutant HIV-1 reverse transcriptase in complexes with ATP and non-nucleoside inhibitor HBY 097. J Mol Biol 365: 77–89.
12. Sarafianos SG, Marchand B, Das K, Himmel DM, Parniak MA, et al. (2009) Structure and function of HIV-1 reverse transcriptase: molecular mechanisms of polymerization and inhibition. J Mol Biol 385: 693–713.
13. Sato H, Tomita Y, Ebisawa K, Hachiya A, Shibamura K, et al. (2001) Augmentation of human immunodeficiency virus type 1 subtype E (CRF01_AE) multiple-drug resistance by insertion of a foreign 11-amino-acid fragment into the reverse transcriptase. J Virol 75: 5604–5613.
14. Sarafianos SG, Clark AD Jr, Das K, Tuske S, Birktoft JJ, et al. (2002) Structures of HIV-1 reverse transcriptase with pre- and post-translocation AZTMP-terminated DNA. Embo J 21: 6614–6624.
15. Ray AS, Murakami E, Basavapathruni A, Vaccaro JA, Ulrich D, et al. (2003) Probing the molecular mechanisms of AZT drug resistance mediated by HIV-1 reverse transcriptase using a transient kinetic analysis. Biochemistry 42: 8831–8841.
16. Marchand B, White KL, Ly JK, Margot NA, Wang R, et al. (2007) Effects of the translocation status of human immunodeficiency virus type 1 reverse transcriptase on the efficiency of excision of tenofovir. Antimicrob Agents Chemother 51: 2911–2919.
17. Furman PA, Fyfe JA, St Clair MH, Weinhold K, Rideout JL, et al. (1986) Phosphorylation of 3′-azido-3′-deoxythymidine and selective interaction of the 5′-triphosphate with human immunodeficiency virus reverse transcriptase. Proc Natl Acad Sci U S A 83: 8333–8337.
18. Vrang L, Bazin H, Remaud G, Chattopadhyaya J, Oberg B (1987) Inhibition of the reverse transcriptase from HIV by 3′-azido-3′-deoxythymidine triphosphate and its threo analogue. Antiviral Res 7: 139–149.
19. Baker D, Sali A (2001) Protein structure prediction and structural genomics. Science 294: 93–96.
20. Kati WM, Johnson KA, Jerva LF, Anderson KS (1992) Mechanism and fidelity of HIV reverse transcriptase. J Biol Chem 267: 25988–25997.
21. Rittinger K, Divita G, Goody RS (1995) Human immunodeficiency virus reverse transcriptase substrate-induced conformational changes and the mechanism of inhibition by nonnucleoside inhibitors. Proc Natl Acad Sci U S A 92: 8046–8049.
22. Goto J, Kataoka R, Muta H, Hirayama N (2008) ASEDock-docking based on alpha spheres and excluded volumes. J Chem Inf Model 48: 583–590.
23. Chen R, Yokoyama M, Sato H, Reilly C, Mansky LM (2005) Human immunodeficiency virus mutagenesis during antiviral therapy: impact of drug-resistant reverse transcriptase and nucleoside and nonnucleoside reverse transcriptase inhibitors on human immunodeficiency virus type 1 mutation frequencies. J Virol 79: 12045–12057.
24. Li Y, Kong Y, Korolev S, Waksman G (1998) Crystal structures of the Klenow fragment of Thermus aquaticus DNA polymerase I complexed with deoxyribonucleoside triphosphates. Protein Sci 7: 1116–1123.
25. Johnson SJ, Taylor JS, Beese LS (2003) Processive DNA synthesis observed in a polymerase crystal suggests a mechanism for the prevention of frameshift mutations. Proc Natl Acad Sci U S A 100: 3895–3900.
26. Yin YW, Steitz TA (2004) The structural mechanism of translocation and helicase activity in T7 RNA polymerase. Cell 116: 393–404.
27. Temiakov D, Patlan V, Anikin M, McAllister WT, Yokoyama S, et al. (2004) Structural basis for substrate selection by t7 RNA polymerase. Cell 116: 381–391.
28. Thompson AA, Albertini RA, Peersen OB (2007) Stabilization of poliovirus polymerase by NTP binding and fingers-thumb interactions. J Mol Biol 366: 1459–1474.
29. Petruska J, Goodman MF, Boosalis MS, Sowers LC, Cheong C, et al. (1988) Comparison between DNA melting thermodynamics and DNA polymerase fidelity. Proc Natl Acad Sci U S A 85: 6252–6256.
30. Ling H, Boudsocq F, Woodgate R, Yang W (2001) Crystal structure of a Y-family DNA polymerase in action: a mechanism for error-prone and lesion-bypass replication. Cell 107: 91–102.
31. Ling H, Boudsocq F, Plosky BS, Woodgate R, Yang W (2003) Replication of a cis-syn thymine dimer at atomic resolution. Nature 424: 1083–1087.
32. Starnes MC, Cheng YC (1989) Human immunodeficiency virus reverse transcriptase-associated RNase H activity. J Biol Chem 264: 7073–7077.
33. Willey RL, Smith DH, Lasky LA, Theodore TS, Earl PL, et al. (1988) In vitro mutagenesis identifies a region within the envelope gene of the human immunodeficiency virus that is critical for infectivity. J Virol 62: 139–147.
34. Shirakawa K, Takaori-Kondo A, Yokoyama M, Izumi T, Matsui M, et al. (2008) Phosphorylation of APOBEC3G by protein kinase A regulates its interaction with HIV-1 Vif. Nat Struct Mol Biol 15: 1184–1191.

Kono et al. Retrovirology 2010, 7:72
http://www.retrovirology.com/content/7/1/72

RETROVIROLOGY

RESEARCH Open Access

Multiple sites in the N-terminal half of simian immunodeficiency virus capsid protein contribute to evasion from rhesus monkey TRIM5α-mediated restriction

Ken Kono[1], Haihan Song[1], Masaru Yokoyama[2], Hironori Sato[2], Tatsuo Shioda[1], Emi E Nakayama[1*]

Abstract

Background: We previously reported that cynomolgus monkey (CM) TRIM5α could restrict human immunodeficiency virus type 2 (HIV-2) strains carrying a proline at the 120th position of the capsid protein (CA), but it failed to restrict those with a glutamine or an alanine. In contrast, rhesus monkey (Rh) TRIM5α could restrict all HIV-2 strains tested but not simian immunodeficiency virus isolated from macaque (SIVmac), despite its genetic similarity to HIV-2.

Results: We attempted to identify the viral determinant of SIVmac evasion from Rh TRIM5α-mediated restriction using chimeric viruses formed between SIVmac239 and HIV-2 GH123 strains. Consistent with a previous study, chimeric viruses carrying the loop between α-helices 4 and 5 (L4/5) (from the 82nd to 99th amino acid residues) of HIV-2 CA were efficiently restricted by Rh TRIM5α. However, the corresponding loop of SIVmac239 CA alone (from the 81st to 97th amino acid residues) was not sufficient to evade Rh TRIM5α restriction in the HIV-2 background. A single glutamine-to-proline substitution at the 118th amino acid of SIVmac239 CA, corresponding to the 120th amino acid of HIV-2 GH123, also increased susceptibility to Rh TRIM5α, indicating that glutamine at the 118th of SIVmac239 CA is necessary to evade Rh TRIM5α. In addition, the N-terminal portion (from the 5th to 12th amino acid residues) and the 107th and 109th amino acid residues in α-helix 6 of SIVmac CA are necessary for complete evasion from Rh TRIM5α-mediated restriction. A three-dimensional model of hexameric GH123 CA showed that these multiple regions are located on the CA surface, suggesting their direct interaction with TRIM5α.

Conclusion: We found that multiple regions of the SIVmac CA are necessary for complete evasion from Rh TRIM5α restriction.

Background

The host range of human immunodeficiency virus type 1 (HIV-1) is very narrow, being limited to humans and chimpanzees [1]. HIV-1 fails to replicate in activated CD4-positive T lymphocytes obtained from Old World monkeys (OWM) such as rhesus (Rh) [2,3] and cynomolgus (CM) monkeys [4,5]. Simian immunodeficiency virus (SIV) isolated from sooty mangabey (SIVsm) and SIV isolated from African green monkey (SIVagm) replicate in their natural hosts [6]. SIV isolated from a macaque monkey (SIVmac) evolved from SIVsm in captive macaques, and replicates efficiently in Rh [2,3] and CM [4,5] monkeys. Human immunodeficiency virus type 2 (HIV-2) is assumed to have originated from SIVsm as the result of zoonotic events involving monkeys and humans [7]. Previous studies have shown that HIV-2 strains vary widely in their ability to grow in cells of OWM such as baboon, and Rh and CM monkeys [8-12].

In 2004, the screening of a Rh cDNA library identified TRIM5α as a factor that confers resistance to HIV-1 infection [13]. Both Rh and CM TRIM5α proteins restrict HIV-1 infection but fail to restrict SIVmac [13,14]. In contrast, human TRIM5α is almost powerless

* Correspondence: emien@biken.osaka-u.ac.jp
[1]Department of Viral Infections, Research Institute for Microbial Diseases, Osaka University, 3-1 Yamada-oka, Suita, Osaka 565-0871, Japan
Full list of author information is available at the end of the article

to restrict the aforementioned viruses, but potently restricts N-tropic murine leukemia viruses (N-MLV) and equine infectious anemia virus [15-17].

TRIM5α is a member of the tripartite motif (TRIM) family of proteins, and consists of RING, B-box 2, coiled-coil, and SPRY (B30.2) domains [18]. Proteins with RING domains possess E3 ubiquitin ligase activity [19]; therefore, TRIM5α was thought to restrict HIV-1 by proteasome-dependent pathways. However, proteasome inhibitors do not affect TRIM5α-mediated HIV-1 restriction, even though HIV-1 late reverse transcribed products are generated normally [20-22]. TRIM5α is thus supposed to use both proteasome-dependent and -independent pathways to restrict HIV-1.

The intact B-box 2 domain is also required for TRIM5α-mediated antiviral activity, since TRIM5α restrictive activity is diminished by several amino acid substitutions in the B-box 2 domain [23,24]. TRIM5α has been shown to form a dimer [25,26], while the B-box 2 domain mediates higher-order self-association of Rh TRIM5α oligomers [27,28]. The coiled-coil domain of TRIM5α is important for the formation of homo-oligomers [29], and the homo-oligomerization of TRIM5α is essential for antiviral activity [30,31]. The SPRY domain is specific for an α-isoform among at least three splicing variants transcribed from the *TRIM5* gene. Soon after the identification of TRIM5α as a restriction factor of Rh, several studies found that differences in the amino acid sequences of the TRIM5α SPRY domain of different monkey species affect the species-specific restriction of retrovirus infection [14,32-39]. Studies on human and Rh recombinant TRIM5αs have shown that the determinant of species-specific restriction against HIV-1 infection resides in variable region 1 (V1) of the SPRY domain [32,33]. In the case of HIV-2 infection, we previously found that three amino acid residues of TFP at the 339th to 341st positions of Rh TRIM5α V1 are indispensable for restricting particular HIV-2 strains that are still resistant to CM TRIM5α [34].

The SPRY domain is thus thought to recognize viral cores. Biochemical studies have shown that TRIM5α associates with CA in detergent-stripped N-MLV virions [40] or with an artificially constituted HIV-1 core structure composed of the capsid-nucleocapsid (CA-NC) fusion protein in a SPRY domain-dependent manner [41]. Ylinen *et al.* mapped one of the determinants of Rh TRIM5α sensitivity to a loop between α-helices 4 and 5 (L4/5) of HIV-2 [42]. In the present study, we found that the 120th amino acid of HIV-2 CA, which is the determinant of CM TRIM5α sensitivity, also contributes to Rh TRIM5α susceptibility. Furthermore, studies on chimeric viruses between Rh TRIM5α-sensitive HIV-2 and -resistant SIVmac revealed that multiple regions in the N-terminal half of SIVmac CA including L4/5 contribute to the escape of SIVmac from Rh TRIM5α.

Methods

DNA constructs

The HIV-2 derivatives were constructed on a background of infectious molecular clone GH123 [43]. Construction of GH123/Q, the mutant GH123 possessing Q at the 120th position of CA protein, and SIVmac239/P, the mutant SIVmac239 possessing P at the 118th position of CA, were described previously [44]. The CA L4/5 of GH123 or GH123/Q was replaced with the corresponding segments of SIVmac239 CA using site-directed mutagenesis with the PCR-mediated overlap primer extension method [45], and the resultant constructs were designated GH123/CypS or GH123/CypS 120Q, respectively. The GH123 derivative with L4/5 of SIVmac239, Q at the 120th, and A at the 179th position of CA (GH123/CypS 120Q 179A) was generated by site-directed mutagenesis on a background of GH123/CypS 120Q.

Chimeric GH123 containing the whole region of SIVmac239 CA (GH/SCA) was generated by site-directed mutagenesis. Restriction enzyme sites *Ngo*M IV and *Xho* I, located in the LTR and p6 cording region, respectively, were used for DNA recombination. To obtain the *Ngo*M IV-*Xho* I fragment containing the CA region, we performed four successive PCR reactions using GH123 and SIVmac239 as templates. The primers used in these reactions were GH114F (5'-TTGGCCGGCACTGG-3'), SCA1For (5'-CCAGTACAACAAATAGG-3'), SCA1 Rev (5'-CCTATTTGTTGTACTGG-3'), SCA2 For (5'-GCTAGATTAATGGCCGAAGCCCTG-3'), SCA2 Rev (5'-CAGGGCTTCGGCCATTAATCTAGC-3'), and 2082R (5'-GACAGAGGACTTGCTGCAC-3').

The first PCR reaction used GH123 as a template and GH114F and GHSCA1 Rev as primers, the second used SIVmac239 as a template and GHSCA1 For and GHSCA2 Rev as primers, and the third used GH123 as a template and GHSCA2 For and 2082R as primers. The resultant 1st, 2nd, and 3rd fragments were used as templates in the fourth reaction with GH114F and 2082R as primers. The resultant *Ngo*M IV-*Xho* I fragment was transferred to GH123. GH/SCA derivatives GH/SCA N-G, GH/SCA VD, GH/SCA CypG, and GH/SCA TE were constructed by site-directed mutagenesis on a GH/SCA background.

To construct GH/NSCG, a GH123 derivative containing the N-terminal half (from 1st to 120th) of SIVmac239CA, we performed three successive PCR reactions. The first used GH/SCA as a template and GH114F and NSCA Rev (5'-GGGATTTTGTTGTCTGTACATCC-3') as primers, the second used GH123 as a

template and NSCA For (5'-GGATGTACAGACAA-CAAAATCCC-3') and 2082R as primers. The resultant 1st and 2nd fragments were used as templates in the third reaction with GH114F and 2082R as primers. The resultant *Ngo*M IV-*Xho* I fragment was transferred to GH123. The GH/NSCG derivative GH/GSG was constructed by site-directed mutagenesis on a GH/NSCG background.

Cells

The 293T (human kidney) and FRhK4 (Rh kidney; American Type Culture Collection, Manassas, VA) were cultured in Dulbecco's modified Eagle medium supplemented with 10% heat-inactivated fetal bovine serum (FBS). MT4, a human CD4 positive T cell line immortalized by human T cell leukemia virus type 1 [46], was maintained in RPMI 1640 medium containing 10% FBS.

Viral propagation

Virus stocks were prepared by transfection of 293T cells with HIV-2 GH123 derivatives using the calcium phosphate co-precipitation method. Viral titers were measured with the p27 RETROtek antigen ELISA kit (ZeptoMetrix, Buffalo, NY).

Recombinant Sendai virus (SeV) carrying Rh, CM, or CM SPRY(-) TRIM5α was described previously [14,34]. Green fluorescence protein (GFP) expressing HIV-1 carrying SIVmac239 L4/5 (HIV-1-L4/5-GFP) was prepared as described previously [47].

Viral infection

MT4 cells (2×10^5) were infected with SeV expressing each of the TRIM5αs, at a multiplicity of infection (MOI) of 10 plaque-forming units (pfu) per cell and incubated at 37°C for 9 h. Cells were then superinfected with 20 ng of p25 of HIV-2 GH123 or derivatives, or 20 ng of p27 of SIVmac239 or derivatives. Culture supernatants were collected periodically, and the levels of p25 or p27 were measured with the RETROtek antigen ELISA kit.

Particle purification and Western blot analysis

Culture supernatant of 293T cells transfected with plasmids encoding HIV-1 NL43 and HIV-2 GH123 derivatives was clarified using low-speed centrifugation. The resultant supernatants were layered onto a cushion of 20% sucrose (made in PBS) and centrifuged at 35,000 rpm for 2 h in a Beckman SW41 rotor. After centrifugation, the virion pellets were resuspended in PBS and applied to sodium dodecyl sulfate-polyacrylamide gel electrophoresis (SDS-PAGE). Virion-associated proteins were transferred to a PVDF membrane. CAs and cyclophilin A (CypA) were visualized with the serum from SIV-infected monkeys or the anti-CypA antibody (Affinity BioReagents, Golden, CO), respectively.

Saturation assay

HIV-2 or SIVmac derivative particles were prepared by co-transfection of the relevant plasmids with one encoding vesicular stomatitis virus glycoprotein (VSV-G) into 293T cells, and culture supernatants were collected two days after transfection. One day before infection, FRhK-4 cells were plated at a density of 2×10^4 cells per well in a 24-well plate. Prior to GFP virus infection, the cells were pretreated for 2 h with 800 ng of p25 of each of HIV-2 or SIVmac derivatives pseudotyped with VSV-G. Immediately after pretreatment, cells were washed and infected with 10 ng of p24 of the HIV-1-L4/5-GFP virus. Then, 2 h after infection, the inoculated GFP viruses were washed and the cells cultivated in fresh media. Two days after infection, GFP-positive cells were counted with a flow cytometer.

Molecular modeling of hexameric HIV-2 CA

The crystal structures of the HIV-2 CA N-terminal domain at a resolution of 1.25Å [PDB: 2WLV] [48], HIV-1 CA C-terminal domain at a resolution of 1.70Å (PDB code: 1A8O) [49], and hexameric HIV-1 CA at a resolution of 1.90Å [PDB:3H47] [50] were taken from the RCSB Protein Data Bank [51]. Three-dimensional (3-D) models of monomeric HIV-2 CA were constructed by the homology modeling technique using 'MOE-Align' and 'MOE-Homology' in the Molecular Operating Environment (MOE) version 2008.1002 (Chemical Computing Group Inc., Quebec, Canada) as described [44,52]. We obtained 25 intermediate models per one homology modeling in MOE, and selected those 3-D models which were intermediate with best scores according to the generalized Born/volume integral methodology [53]. The final 3-D models were thermodynamically optimized by energy minimization using an AMBER99 force field [54] combined with the generalized Born model of aqueous solvation implemented in MOE [55]. Physically unacceptable local structures of the optimized 3-D models were further refined on the basis of evaluation by the Ramachandran plot using MOE. The structures of hexameric HIV-2 CA were generated from the monomeric structures by MOE on the basis of the assembly information of hexameric HIV-1 CA crystal structures [50].

Results

The L4/5 loop of SIVmac239 CA and Q and A at the 120th and 179th positions of CA are not sufficient for HIV-2 to evade Rh TRIM5α-mediated restriction

Previously, we evaluated the antiviral effect of CM and Rh TRIM5α and found that CM TRIM5α could restrict

HIV-2 GH123 carrying P at the 120th position of CA, but failed to restrict the HIV-2 GH123 mutant in which P was replaced with Q (GH123/Q) [44] (Figure 1A). In contrast, Rh TRIM5α could restrict both viruses [34] (Figure 2A and 2B). Although CA of HIV-2 GH123 and SIVmac239 share more than 87% amino acid identity (Figure 1B), CM and Rh TRIM5αs failed to restrict SIVmac239 (Figure 2C).

Since wild type SIVmac239 possesses Q at the 118th position of CA (analogous to the 120th position of GH123 CA), we constructed mutant SIVmac239 carrying P at the 118th position (SIVmac239/P), and found

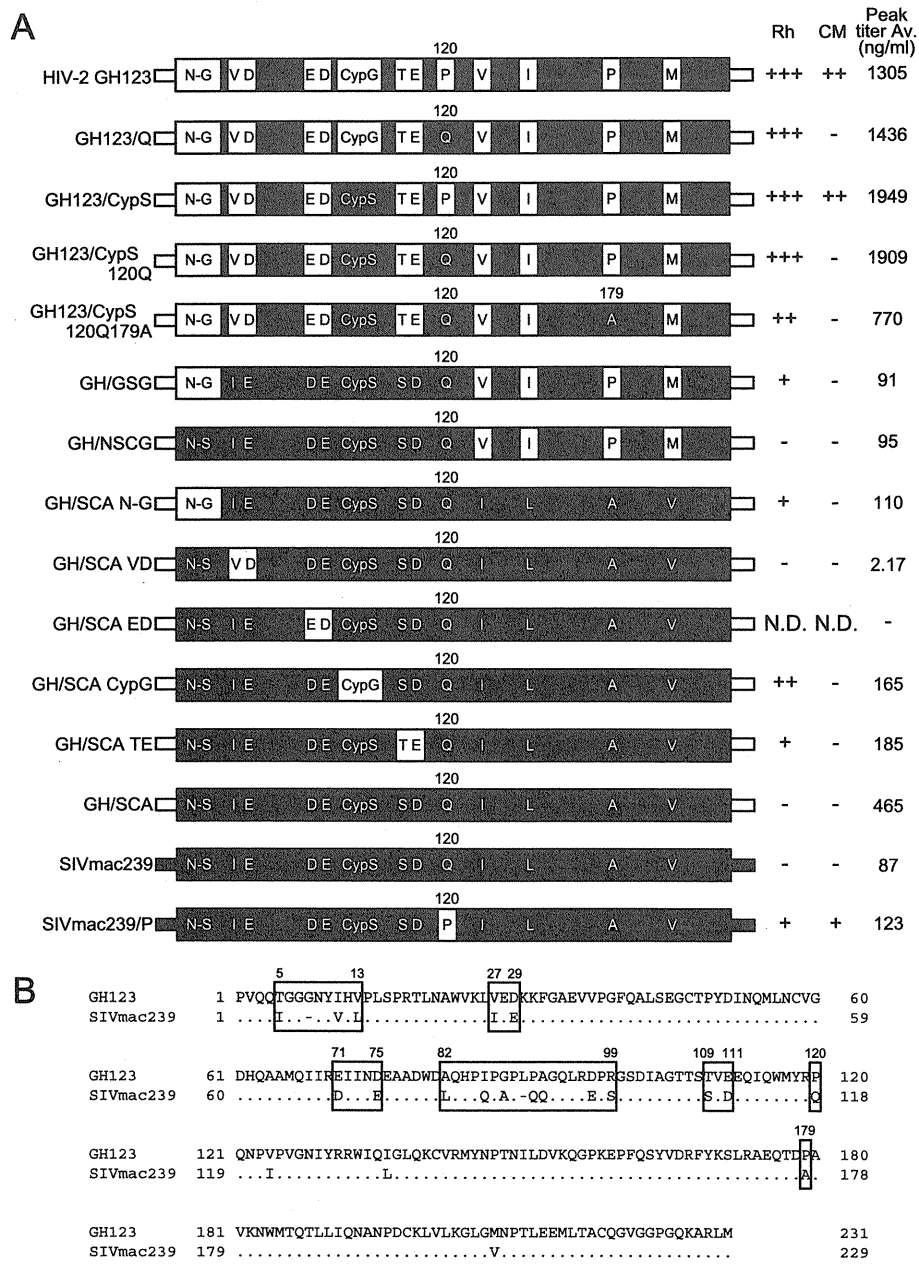

Figure 1 Schematic representation of chimeric viral CAs. (A) White and black bars denote HIV-2 GH123 and SIVmac239 sequences, respectively. +++, ++, +, and - denote more than 1000-fold, 100- to 1000-fold, 5- to 100-fold, and less than 5-fold suppression of viral growth, respectively, compared with viral growth in the presence of negative control CM SPRY(-) TRIM5α on day 6. Peak titer Av. denotes average titers in the presence of CM SPRY(-) TRIM5α on day 6 of two independent experiments. (B) Alignments of amino acid sequences of GH123 and SIVmac239 CAs. Dots denote amino acid residues identical to one of the GH123 CA and dashes denote lack of an amino acid residue present in GH123 CA. Boxes show the regions replaced between GH123 and SIVmac239.

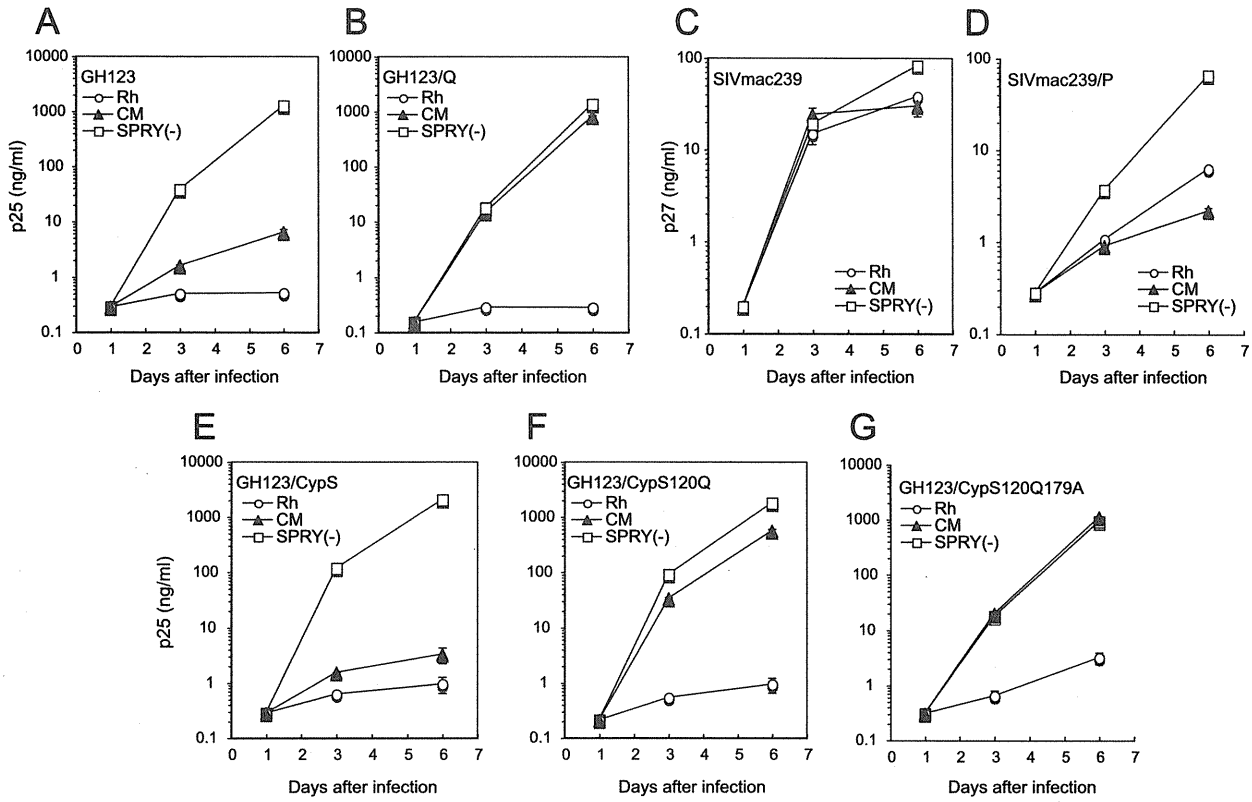

Figure 2 MT4 cells were infected with recombinant SeV expressing Rh (white circles), CM (black triangles), or CM SPRY(-) (white squares) TRIM5α. Nine hours after infection, cells were superinfected with GH123, SIVmac239 or their derivative viruses. Culture supernatants were separately assayed for levels of p25 from GH123 or p27 from SIVmac239. Error bars show actual fluctuations between levels of p25 or p27 in duplicate samples. A representative of two independent experiments is shown.

that CM and Rh TRIM5αs could restrict the mutant virus [44] (Figure 2D). These results indicate that Q at the 118th position of CA is required to evade restriction by CM and Rh TRIM5αs, although Rh TRIM5α could restrict GH123/Q. In the case of Rh TRIM5α, it has been reported that Rh TRIM5α sensitivity determinants lie in the loop between α-helices 4 and 5 of CA protein, equivalent to the cyclophilin A (CypA) binding loop of HIV-1 [42]. This conclusion was made after Rh TRIM5α restricted SIVmac-based SIV H2L in which the L4/5 was replaced with that of HIV-2. However, when we constructed a GH123 derivative in which L4/5 was replaced with that of SIVmac239 (GH123/CypS), the reciprocal virus of SIV H2L, we found that Rh TRIM5α still restricted this virus very well (Figure 2E), indicating that SIVmac239 L4/5 alone is not sufficient for HIV-2 to evade Rh TRIM5α restriction.

We then constructed a GH123 derivative with L4/5 of SIVmac239 (CypS) and Q at the 120th position of CA (GH123/CypS 120Q). Contrary to our expectations, Rh TRIM5α still fully restricted this virus (Figure 2F). Since we previously found that the amino acid change at the 179th position of HIV-2 CA correlated with plasma viral load in infected individuals [56], we next replaced P at the 179th position of GH123/CypS 120Q CA with alanine (A) of SIVmac239 CA analogous to the 179th position of GH123 CA to generate GH123/CypS 120Q179A. However, Rh TRIM5α also completely restricted this virus (Figure 2G). The peak titers of GH123/CypS 120Q and GH123/CypS 120Q179A in cells expressing Rh TRIM5α were approximately 1000 times (+++ in Figure 1) and 300 times (++ in Figure 1), respectively, lower than those in cells expressing CM TRIM5α lacking the SPRY domain, CM SPRY (-) TRIM5α, a negative control for functional TRIM5α (Figure 2F and 2G). Although this result suggests that the 179th amino acid slightly contributes to evade Rh TRIM5α, it is clear that L4/5 of SIVmac239 CA and Q at the 120th and A at the 179th positions of CA were insufficient to evade Rh TRIM5α-mediated restriction.

In the case of CM TRIM5α, viruses carrying P at the 120th position (GH123, GH123/CypS, and SIVmac239/P) were restricted by CM TRIM5α, whereas all other viruses bearing Q (GH123/Q, GH123/CypS 120Q, GH123/CypS 120Q179A, and SIVmac239) were not (Figures 1 and 2). These results are in good agreement

with our previous conclusion that glutamine at the 120th position of HIV-2 CA alone is sufficient to evade CM TRIM5α restriction [34,44].

The N-terminal half of SIVmac239 CA is sufficient to evade Rh TRIM5α

To confirm that CA contains all determinants for restriction by Rh TRIM5α, we constructed a chimeric GH123 containing the whole region of SIVmac239 CA (GH/SCA). This virus could grow in the presence and absence of Rh TRIM5α (Figures 1 and 3A), clearly excluding the possibility that some of the determinants lie outside the CA. We then generated a chimeric GH123 containing the N-terminal half (from the 1st to 120th) of SIVmac239 CA (GH/NSCG) to further narrow down the determinant for restriction by Rh TRIM5α. Although GH/NSCG grew to lower titers than GH/SCA, even in the absence of Rh TRIM5α, this virus could also grow in the presence of Rh TRIM5α (Figures 1 and 3B). These results suggest that the N-terminal half of SIVmac239 CA is almost sufficient to evade Rh TRIM5α, even though the 179th amino acid of the C-terminal half possessed a slight effect of restriction.

Multiple sites in the N-terminal half of SIVmac239 CA contribute to evasion from restriction by Rh TRIM5α

In the N-terminal half of GH123 CA, 19 amino acid residues differ from those of SIVmac239. We grouped these differences into six regions as shown by boxes in Figure 1B, and evaluated their contribution to evasion from Rh TRIM5α by replacing each region of GH/SCA with the corresponding region of GH123. Rh TRIM5α completely restricted the GH/SCA derivative with the GH123 L4/5 (CypG) (GH/SCA CypG) (Figures 1 and 3C), consistent with a previous study [42]. Rh TRIM5α moderately restricted the GH/SCA derivative with threonine (T) and glutamic acid (E) of GH123 at the 109th and 111th positions, respectively (GH/SCA TE) (Figures 1 and 3D). These results suggest that not only L4/5 but also the 107th and 109th of amino acid residues of SIVmac239 CA (analogous to the 109th and 111th of GH123 CA) contribute to evasion from restriction by Rh TRIM5α.

Moreover, Rh TRIM5α slightly but significantly restricted the GH/SCA derivative with the GH123 N-terminal portion from the 5th to 13th amino acid residues (N-G) (GH/SCA N-G) (Figures 1 and 3E) ($p < 0.05$, t-test, n = 4), indicating that the SIVmac239 N-terminal portion from 5th to 12th (N-S) (analogous to N-G) is also important in evasion from Rh TRIM5α. Consistent with this result, Rh TRIM5α which failed to restrict GH/NSCG, could restrict the GH/NSCG

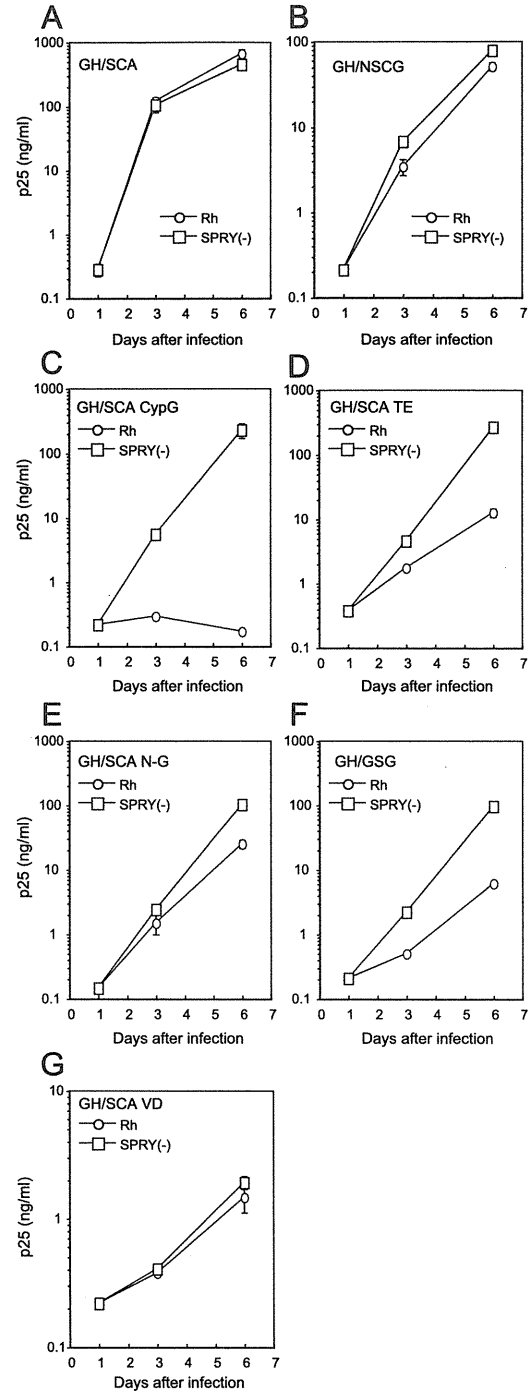

Figure 3 MT4 cells were infected with recombinant SeV expressing Rh (white circles) or CM SPRY(-) (white squares) TRIM5α. Nine hours after infection, cells were superinfected with GH/SCA (A), GH/NSCG (B) or GH/SCA derivatives (C-G). Culture supernatants were separately assayed for levels of p25. Error bars show actual fluctuations between levels of p25 in duplicate samples. A representative of two independent experiments is shown.

derivative with N-G (GH/GSG) (Figures 1 and 3F). On the other hand, Rh TRIM5α failed to restrict the GH/SCA derivative with the valine (V) and aspartic acid (D) of GH123 at the 27th and 29th positions, respectively (GH/SCA VD) (Figures 1 and 3G). It should be noted, however, that the growth capability of GH/SCA VD in MT4 cells was extremely low even in the absence of TRIM5α (Figure 3G), and further studies are necessary to address the contribution of this region to viral sensitivity to Rh TRIM5α. Similarly, the GH/SCA derivative with glutamic acid (E) and D of GH123 at the 71st and 75th positions (GH/SCA ED) (Figure 1) did not grow in MT4 cells expressing CM SPRY (-) TRIM5α, thus, we were unable to evaluate the effect of these sites. Taken together, we conclude that multiple sites in the N-terminal half of SIVmac239 CA (N-S, CypS (L4/5), and the 107th, 109th, and 118th amino acid residues) contribute to evasion from restriction by Rh TRIM5α.

We previously reported that a mutant CM TRIM5α possessing TFP instead of Q at the 339th position (CM Q-TFP TRIM5α) potently restricted GH123/Q [34]. In the present study, CM Q-TFP TRIM5α showed nearly the same spectrum of virus restriction as Rh TRIM5α as it completely restricted GH/SCA CypG, moderately restricted GH/SCA TE and SIVmac239/P, and only slightly restricted GH/SCA N-G (data not shown). These results indicate that the virus restriction specificity of Rh TRIM5α is highly dependent on the three amino acid residues 339th-TFP-341st.

CypA was not incorporated into GH123, SIVmac239 or their derivative virus particles

It has been reported that CypA was incorporated into group M HIV-1, but not HIV-2 or SIVmac particles [57]. To confirm that the replacement of CA between GH123 and SIVmac239 did not augment CypA incorporation, we performed Western blot analysis of viral particles from GH123, SIVmac239, and their derivatives. As shown in Figure 4 (upper panel), CypA proteins were clearly detected in the particles of HIV-1 NL43 but not in those of GH123, GH/SCA, GH/SCA CypG or SIVmac239, although the amount of their CA proteins was almost comparable (Figure 4, lower panel). This result indicates that the replacement between GH123 and SIVmac239 did not augment their CypA incorporation ability.

Rh TRIM5α-resistant HIV-2 derivative virions showed impaired saturation activity to TRIM5α in Rh cells

It is known that TRIM5α-mediated restriction of retroviral infection is saturated when cells are exposed to high doses of restriction-sensitive viral particles [58-61]. To determine whether the amino acid substitutions we generated would affect the viral ability to saturate

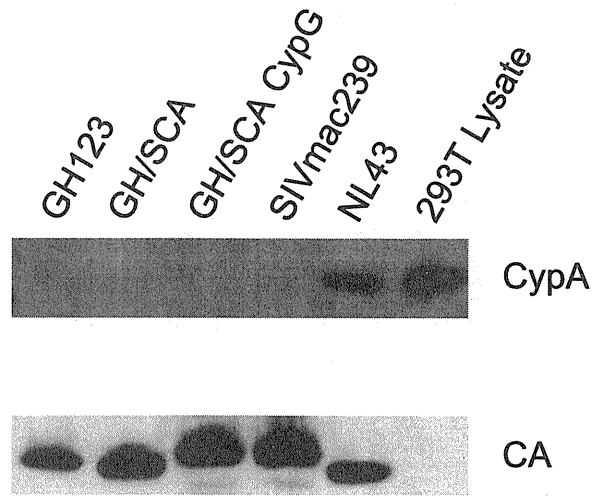

Figure 4 Western blot analysis of CA and CypA in particles of GH123, SIVmac239 and their derivatives. Viral particles from HIV-1 NL43, HIV-2 GH123, SIVmac239, and their derivatives were purified by ultracentrifugation through a 20% sucrose cushion. A total of 120 ng of p24 of HIV-1, p25 of HIV-2 GH123 derivatives or p27 of SIVmac239 derivatives was applied for gel electropholesis. Cyp A (upper panel) and CA (lower panel) were visualized by Western blotting (WB) using an anti-CypA antibody and serum from a SIV-infected monkey, respectively.

TRIM5α restriction, Rh FRhK4 cells were pre-treated with equal amounts of VSV-G pseudotyped HIV-2 GH123, SIVmac239, and their derivative viruses. The pretreated cells were then infected with VSV-G pseudotyped GFP expressing HIV-1 carrying SIVmac239 L4/5 (HIV-1-L4/5S-GFP) [47], since we wanted to exclude the effects of endogenous CypA on GFP-expressing virus in FRhK4 cells. The susceptibility of particle-treated cells to virus infection was determined by the percentage of GFP-positive cells.

Cells treated with HIV-2 GH123 particles showed enhanced susceptibility to HIV-1 infection compared with non-treated cells (Figure 5), demonstrating that TRIM5α in FRhK4 cells was saturated by the high dose of the particles. In contrast, cells treated with SIVmac239 particles showed very low levels of enhancement. Cells treated with particles carrying GH123/Q showed similar levels of enhanced susceptibility to HIV-1 infection to those of HIV-2 GH123, while cells treated with particles of GH123/CypS, GH123/CypS 120Q, GH/SCA CypG or SIVmac239/P showed intermediate levels of enhancement (Figure 5).

On the other hand, cells treated with particles carrying GH/NSCG, GH/SCA, and GH/SCA N-G showed similar levels of enhancement of HIV-1 susceptibility to those of SIVmac239 (Figure 5). These results are roughly consistent with our data shown in Figures 2 and 3, but there are two differences. First, Rh TRIM5α could

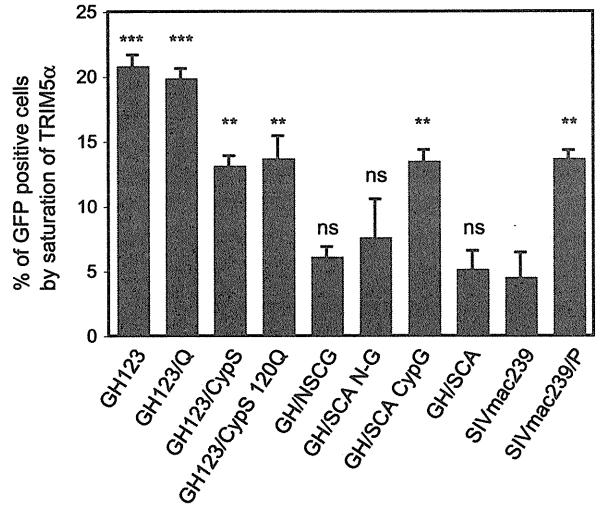

Figure 5 Activity of GH123, SIVmac239, and their derivatives to saturate TRIM5α in Rh cells. (A) Rh FRhK-4 cells were pretreated with equal amounts of VSV-G pseudotyped particles (800 ng of p25 or p27) of GH123, GH123/Q, GH123/CypS, GH123/CypS 120Q, GH/NSCG, GH/SCA N-G, GH/SCA CypG, GH/SCA, SIVmac239 or SIVmac239/P for 2 h. Cells were then infected with the VSV-G pseudotyped GFP-expressing HIV-1 vector carrying SIVmac L4/5. Data from triplicate samples (means ± SD) expressed as % GFP positive cells subtracted with the value of mock-treated cells (24.88%) are shown. Statistical significance of differences was calculated using the *t*-test. Asterisks above bars show differences between indicated viruses and SIVmac239. ***, $P < 0.001$; **, $P < 0.01$; ns, not significant. The statistical significance of differences between GH123 and GH123/CypS and that between GH123 and GH/SCA CypG were both < 0.001.

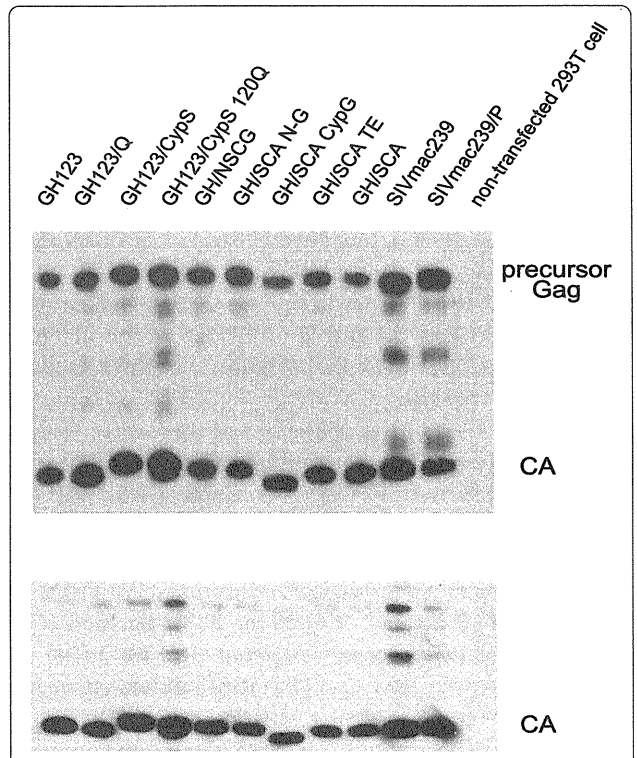

Figure 6 Western blot analysis of lysates of viral producer cells and viral particles. Viral proteins in the lysate of equal number of viral producer cells (upper panel) and particle fraction of equal volume of culture supernatant of viral producer cells (lower panel) were visualized by WB using serum from an SIV-infected monkey.

completely restrict GH123/CypS and GH123/CypS 120Q (Figure 2), while particles of these viruses showed decreased levels of enhancement compared with those of GH123 or GH123/Q (Figure 5). Second, Rh TRIM5α could slightly restrict GH/SCA N-G (Figure 3E), while particles of this virus failed to saturate Rh TRIM5α (Figure 5). Although the precise reasons for these differences are unclear at present, similar differences were previously reported in HIV-1 CA mutant constructs, and might be due to differences in core stability among mutant viral particles [62]. Nevertheless, our data in Figure 5 clearly indicate the importance of L4/5 (compare GH123 with GH123/CypS, GH/SCA with GH/SCA CypG) and other CA regions (compare GH123 with GH/SCA CypG, SIVmac239 with SIVmac239/P) in the viral ability to saturate TRIM5α in Rh FRhK4 cells, and suggest that the multiple sites in the N-terminal half of GH123 CA affect its binding to Rh TRIM5α.

Finally, we checked viral release and maturation/processing of GH123, SIVmac239, and their derivative viruses by a western blot for the lysate of viral producer cells (Figure 6, upper panel) and viral particles (Figure 6, lower panel), since viral maturation is essential for TRIM5α recognition. CA proteins in the cells and released viral particles were clearly detected. CAs with SIVmac239 L4/5 showed slightly reduced mobility compared with those with GH123 L4/5. Although there were small differences in the amounts of CA among viruses tested, there was no difference in the ratio of intracellular CA to those in the released viral particles. It should be also mentioned that there was no difference in the ratio of Gag precursors to processed CA in the viral producer cells. These results indicated that viral release and maturation/processing of the derivative viruses occurred normally.

Structural model of HIV-2 GH123 CA

To gain a structural insight into the mechanisms by which Rh TRIM5α recognizes HIV-2 CA, three-dimensional (3-D) models of monomeric and hexameric HIV-2 GH123 CA were constructed using homology-modeling based on the crystal structures of the HIV-2 CA N-terminal domain [48], HIV-1 CA C-terminal domain [49], and the hexameric HIV-1 CA [50]. All amino acid residues conferring sensitivity to Rh TRIM5α restriction (N-G, CypG (L4/5), the 109th T, 111th E, and 120th P) are located on the surface of CA

(Figure 7A, C and 7D), suggesting that these positions are involved in interaction with Rh TRIM5α. On the other hand, amino acid residues that impaired viral growth in the absence of TRIM5α (27^{th} V, 29^{th} D, 71^{st} E, and 75^{th} D) are located on the side of CA (Figure 7A and 7D). Although we were unable to determine the effect of these amino acid residues on viral sensitivity to Rh TRIM5α restriction, the structural models suggest that these sites are buried inside multimerized CA. It is therefore unlikely that they are involved in the direct interaction of CA with Rh TRIM5α.

Discussion

A previous study on the recombination between HIV-2 ROD and SIVmac showed that the CA region corresponding to the CypA binding loop of HIV-1 (L4/5) is

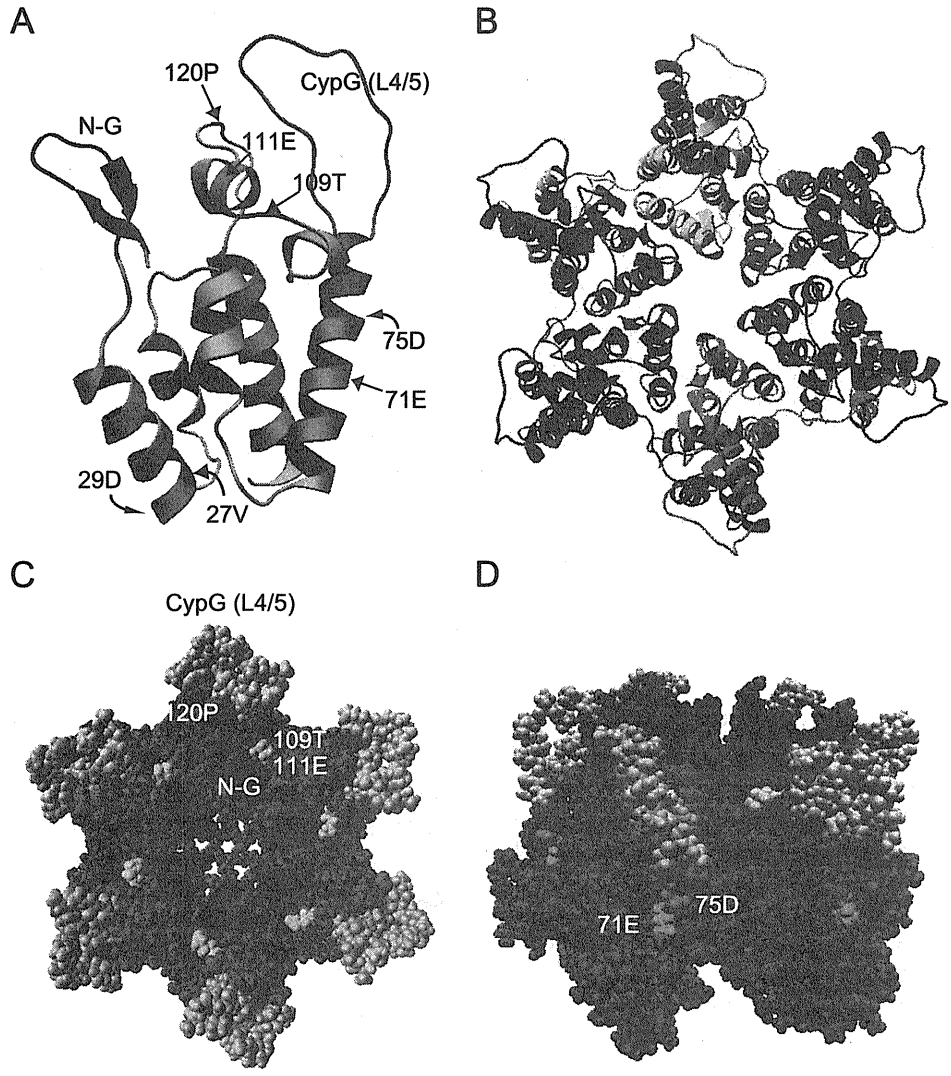

Figure 7 Three-dimensional structural models of GH123 CA. (A) Structure of the N-terminal half of CA monomer. The model was constructed by homology-modeling using "MOE-Align" and "MOE-Homology" in the Molecular Operating Environment (MOE) as described previously [73,74]. N-G, dark purple; the 27^{th}V and the 29^{th}D, pink; Cyp G (L4/5), orange; the 71^{st}E, green; the 75^{th}D, light purple; the 109^{th} T, dark blue; the 111^{th} E, light blue; and the 120^{th} P, red. The structure of CA hexamer from the top (B and C) and side (D) is shown.

the determinant for susceptibility to Rh TRIM5α [42]. A subsequent study on HIV-1 and SIVagmTAN showed that the loop between helices 6 and 7 (L6/7) also contributes to Rh TRIM5α susceptibility [63]. In the present study, we showed that the L4/5 and the 120th amino acids located in L6/7 were required but not sufficient for HIV-2 to evade Rh TRIM5α-mediated restriction.

In addition to L4/5 and L6/7, we found that the N-terminal portion (from the 5th to 12th amino acid residues), and 107th and 109th amino acid residues in α-helix 6 of SIVmac239 CA are required for Rh TRIM5α evasion. The 3-D models of CA showed that the analogous regions of GH123 CA are located on the surface of the CA core structure, suggesting that these sites are involved in the direct interaction of CA with Rh TRIM5α. Our results are in good agreement with a previous report in which the HIV-1 derivative with an entire CA and Vif of SIVmac239 could replicate in Rh cells [64]. In addition, we observed that the HIV-1 derivative with L4/5 and L6/7 of CA and Vif of SIVmac239 (NLScaVR6/7S) that replicates in CM cells [47] failed to replicate in Rh cells (Kuroishi et al., unpublished data).

The growth ability of GH123 was higher than that of SIVmac239 in SeV-infected MT4 cells, but that of many GH123 derivatives with SIVmac239 CA sequences was lower than that of the parental GH123 and comparable with that of SIVmac239 (Figures 1, 2, and 3). However, GH/SCA VD replicated very poorly and GH/SCA ED did not replicate at all. These results were reproducible using the viruses produced with independent plasmid clones, after which Gag processing of these viruses occurred normally (data not shown). As shown in Figure 7, the 27th V and 29th D are in α-helix 1, and the 71st E and 75th D are in α-helix 4. It is possible that the amino acid changes at these sites are harmful for the formation of a multimerized viral core. Supporting this notion, the 27th V and 71st E are highly conserved among different HIV-2 strains in the Los Alamos sequence database. Furthermore, the 71st E and 75th D are located on the lateral side of the CA hexametric structure (Figure 7D), and thus it is possible that these amino acid residues associate with the neighboring CA hexamer. It is thus interesting to know the impact of such amino acid changes on viral core formation.

It has been reported that the CypA-CA interaction renders HIV-1 more susceptible to Rh TRIM5α restriction [65-68]. We found that HIV-2 CA L4/5 corresponding to the CypA binding loop of HIV-1 had the biggest impact on Rh TRIM5α susceptibility, although we could not detect CA-CypA binding (Figure 4). Braaten *et al.* also reported that neither HIV-2 nor SIV recruits CypA into their cores, and that drugs that block CA-CypA interaction have no effect on the titers of these viruses [57]. CA crystal structures of human T-cell lymphotropic virus type 1 [PDB: 1QRJ] [69] and equine infectious anemia virus [PDB: 1EIA] [70] possess an exposed loop directed to the surface of the CA core structure, similar to the HIV-1 CypA binding loop, while retroviruses such as B-tropic murine leukemia virus [PDB: 3BP9] [71] and Jaagsiekte sheep retrovirus [PDB: 2V4X] [72] do not. It is reasonable to assume that this HIV-2 loop would interact with certain host factors other than CypA, and consequently is an attractive target for TRIM5α.

The differences in the L4/5 amino acid sequence among different strains of HIV-2, SIVmac, and SIVsmm are shown in Figure 8. Of these, SIVmac-specific amino acid residues are the 88th A, 90th-QQΔ-92nd, and 99th S (Figure 8 boxes). Ylinen *et al.* reported that SIVmac QQ LPA, the mutant SIVmac containing HIV-2-specific LPA instead of QQ at the 90th to 92nd positions, was still not restricted by Rh TRIM5α [42], suggesting that the 88th and 99th amino acids or all amino acid substitutions in L4/5 between SIVmac and HIV-2 are involved in resistance to Rh TRIM5α restriction.

We previously reported that the TFP motif in the SPRY domain of Rh TRIM5α is important in restriction

```
                    82                                  99
H2A GH123           AQHPIPGPLPAGQLRDPR
H2A ROD             V.....|.|...|....E.|.
H2A UC2             ......|.|...|......|.
H2A ALI             VA....|.|...|....E.|.
H2A D194            ......|.|...|......|.
H2A BEN             S.....|.|...|......|.
H2B KR020           V.....|.|...|......|.
H2B UC1             Q.....|.|...|......|.
H2U 12034           T...NQ|.|P..|....E.|.

MAC 239             L...Q.|A|QQ-|....E.|S
MAC 95058           L...Q.|A|QQ-|......|S
MAC NN142           L...QQ|A|QQ-|......|S
MAC MNE8            L...QQ|A|QQ-|......|S

SMM PGM53           L...Q.|.|I.|......|.
SMM SME543          L...Q.|.|...|....E.|.
SMM PBJ14           L...Q.|.|I.P|....E.|.
```

Figure 8 Alignments of amino acid sequences of the CA L4/5 region of HIV-2, SIVmac, and SIVsmm selected from the Los Alamos databases. Dots denote the amino acid identical to one of the GH123 CA and dashes denote lack of an amino acid residue that is present in GH123 and other viruses. Boxes show the site of SIVmac-specific amino acid residues. H2A, B, and U represent HIV-2 group A, B, and U, respectively. MAC represents SIVmac, and SMM denotes SIVsmm.

of HIV-2 strains that are not restricted by CM TRIM5α [34]. In the present study, we confirmed that this motif is both necessary and sufficient to restrict various HIV-2-SIVmac chimeras that are restricted by Rh TRIM5α. If the TFP motif in the SPRY domain of Rh TRIM5α is directly involved in interaction with viral CA, it is not clear why multiple regions of SIVmac239 are necessary for evasion from TRIM5α with a TFP motif. We previously constructed the 3-D structural model of the SPRY domain [36] using homology modeling. It would therefore be of interest to construct a 3-D binding model of CA and TRIM5α, and to understand how the 339th-TFP-341st motif of Rh TRIM5α affects recognition of the CAs that differ at multiple positions.

Conclusion

We found that multiple regions of the SIVmac CA, not only L4/5 and the 118th amino acid but also the N-terminal portion (from the 5th to 12th amino acid residues), and the 107th and 109th amino acid residues, are necessary for complete evasion from Rh TRIM5α restriction.

Acknowledgements

We thank Ayumu Kuroishi for providing a saturation assay protocol, Tadashi Miyamoto for helping with experiments, and Setsuko Bandou and Noriko Teramoto for their assistance. This work was supported by grants from the Health Science Foundation, the Ministry of Education, Culture, Sports, Science, and Technology, the Ministry of Health, Labour and Welfare, Japan, and the Japan Society for the Promotion of Science.

Author details

[1]Department of Viral Infections, Research Institute for Microbial Diseases, Osaka University, 3-1 Yamada-oka, Suita, Osaka 565-0871, Japan. [2]Laboratory of Viral Genomics, Pathogen Genomics Center, National Institute of Infectious Diseases, Gakuen 4-7-1, MusashiMurayama-shi, Tokyo, 208-0011, Japan.

Authors' contributions

KK and HS performed experiments. EEN and TS participated in its design. MY and HS carried out computational analysis. KK, EEN, HS and TS drafted the manuscript. All authors read and approved the final manuscript.

Authors' information

KK is a research fellow of the Japan Society for the Promotion of Science. HS was a PhD student of Osaka University. HS is a chief of Laboratory of Viral Genomics, Pathogen Genomics Center, National Institute of Infectious Diseases, Japan; and MY is a staff of this laboratory. TS is a professor, and EEN is an assistant professor of Research Institute for Microbial Diseases, Osaka University.

Competing interests

The authors declare that they have no competing interests.

Received: 9 June 2010 Accepted: 8 September 2010
Published: 8 September 2010

References

1. Gao F, Bailes E, Robertson DL, Chen Y, Rodenburg CM, Michael SF, Cummins LB, Arthur LO, Peeters M, Shaw GM, Sharp PM, Hahn BH: **Origin of HIV-1 in the chimpanzee Pan troglodytes troglodytes.** *Nature* 1999, **397**:436-441.
2. Shibata R, Sakai H, Kawamura M, Tokunaga K, Adachi A: **Early replication block of human immunodeficiency virus type 1 in monkey cells.** *J Gen Virol* 1995, **76(Pt 11)**:2723-2730.
3. Himathongkham S, Luciw PA: **Restriction of HIV-1 (subtype B) replication at the entry step in rhesus macaque cells.** *Virology* 1996, **219**:485-488.
4. Akari H, Mori K, Terao K, Otani I, Fukasawa M, Mukai R, Yoshikawa Y: **In vitro immortalization of Old World monkey T lymphocytes with Herpesvirus saimiri: its susceptibility to infection with simian immunodeficiency viruses.** *Virology* 1996, **218**:382-388.
5. Akari H, Nam KH, Mori K, Otani I, Shibata H, Adachi A, Terao K, Yoshikawa Y: **Effects of SIVmac infection on peripheral blood CD4+CD8+ T lymphocytes in cynomolgus macaques.** *Clin Immunol* 1999, **91**:321-329.
6. VandeWoude S, Apetrei C: **Going wild: lessons from naturally occurring T-lymphotropic lentiviruses.** *Clin Microbiol Rev* 2006, **19**:728-762.
7. Hahn BH, Shaw GM, De Cock KM, Sharp PM: **AIDS as a zoonosis: scientific and public health implications.** *Science* 2000, **287**:607-614.
8. Castro BA, Nepomuceno M, Lerche NW, Eichberg JW, Levy JA: **Persistent infection of baboons and rhesus monkeys with different strains of HIV-2.** *Virology* 1991, **184**:219-226.
9. Fujita M, Yoshida A, Sakurai A, Tatsuki J, Ueno F, Akari H, Adachi A: **Susceptibility of HVS-immortalized lymphocytic HSC-F cells to various strains and mutants of HIV/SIV.** *Int J Mol Med* 2003, **11**:641-644.
10. Castro BA, Barnett SW, Evans LA, Moreau J, Odehouri K, Levy JA: **Biologic heterogeneity of human immunodeficiency virus type 2 (HIV-2) strains.** *Virology* 1990, **178**:527-534.
11. Locher CP, Witt SA, Herndier BG, Abbey NW, Tenner-Racz K, Racz P, Kiviat NB, Murthy KK, Brasky K, Leland M, Levy JA: **Increased virus replication and virulence after serial passage of human immunodeficiency virus type 2 in baboons.** *J Virol* 2003, **77**:77-83.
12. Locher CP, Blackbourn DJ, Herndier BG, Reyes-Teran G, Barnett SW, Murthy KK, Levy JA: **Transient virus infection and pathogenesis of a new HIV type 2 isolate, UC12, in baboons.** *AIDS Res Hum Retroviruses* 1998, **14**:79-82.
13. Stremlau M, Owens CM, Perron MJ, Kiessling M, Autissier P, Sodroski J: **The cytoplasmic body component TRIM5alpha restricts HIV-1 infection in Old World monkeys.** *Nature* 2004, **427**:848-853.
14. Nakayama EE, Miyoshi H, Nagai Y, Shioda T: **A specific region of 37 amino acid residues in the SPRY (B30.2) domain of African green monkey TRIM5alpha determines species-specific restriction of simian immunodeficiency virus SIVmac infection.** *J Virol* 2005, **79**:8870-8877.
15. Hatziioannou T, Perez-Caballero D, Yang A, Cowan S, Bieniasz PD: **Retrovirus resistance factors Ref1 and Lv1 are species-specific variants of TRIM5alpha.** *Proc Natl Acad Sci USA* 2004, **101**:10774-10779.
16. Keckesova Z, Ylinen LM, Towers GJ: **The human and African green monkey TRIM5alpha genes encode Ref1 and Lv1 retroviral restriction factor activities.** *Proc Natl Acad Sci USA* 2004, **101**:10780-10785.
17. Perron MJ, Stremlau M, Song B, Ulm W, Mulligan RC, Sodroski J: **TRIM5alpha mediates the postentry block to N-tropic murine leukemia viruses in human cells.** *Proc Natl Acad Sci USA* 2004, **101**:11827-11832.
18. Reymond A, Meroni G, Fantozzi A, Merla G, Cairo S, Luzi L, Riganelli D, Zanaria E, Messali S, Cainarca S, Guffanti A, Minucci S, Pelicci PG, Ballabio A: **The tripartite motif family identifies cell compartments.** *Embo J* 2001, **20**:2140-2151.
19. Jackson PK, Eldridge AG, Freed E, Furstenthal L, Hsu JY, Kaiser BK, Reimann JD: **The lore of the RINGs: substrate recognition and catalysis by ubiquitin ligases.** *Trends Cell Biol* 2000, **10**:429-439.
20. Anderson JL, Campbell EM, Wu X, Vandegraaff N, Engelman A, Hope TJ: **Proteasome inhibition reveals that a functional preintegration complex intermediate can be generated during restriction by diverse TRIM5 proteins.** *J Virol* 2006, **80**:9754-9760.
21. Wu X, Anderson JL, Campbell EM, Joseph AM, Hope TJ: **Proteasome inhibitors uncouple rhesus TRIM5alpha restriction of HIV-1 reverse transcription and infection.** *Proc Natl Acad Sci USA* 2006, **103**:7465-7470.
22. Maegawa H, Miyamoto T, Sakuragi J, Shioda T, Nakayama EE: **Contribution of RING domain to retrovirus restriction by TRIM5alpha depends on combination of host and virus.** *Virology* 2010, **399**:212-220.
23. Javanbakht H, Diaz-Griffero F, Stremlau M, Si Z, Sodroski J: **The contribution of RING and B-box 2 domains to retroviral restriction mediated by monkey TRIM5alpha.** *J Biol Chem* 2005, **280**:26933-26940.
24. Diaz-Griffero F, Kar A, Perron M, Xiang SH, Javanbakht H, Li X, Sodroski J: **Modulation of retroviral restriction and proteasome inhibitor-resistant**

turnover by changes in the TRIM5alpha B-box 2 domain. *J Virol* 2007, **81**:10362-10378.

25. Kar AK, Diaz-Griffero F, Li Y, Li X, Sodroski J: **Biochemical and biophysical characterization of a chimeric TRIM21-TRIM5alpha protein.** *J Virol* 2008, **82**:11669-11681.
26. Langelier CR, Sandrin V, Eckert DM, Christensen DE, Chandrasekaran V, Alam SL, Aiken C, Olsen JC, Kar AK, Sodroski JG, Sundquist WI: **Biochemical characterization of a recombinant TRIM5alpha protein that restricts human immunodeficiency virus type 1 replication.** *J Virol* 2008, **82**:11682-11694.
27. Li X, Sodroski J: **The TRIM5alpha B-box 2 domain promotes cooperative binding to the retroviral capsid by mediating higher-order self-association.** *J Virol* 2008, **82**:11495-11502.
28. Diaz-Griffero F, Qin XR, Hayashi F, Kigawa T, Finzi A, Sarnak Z, Lienlaf M, Yokoyama S, Sodroski J: **A B-box 2 Surface Patch Important for TRIM5 {alpha} Self-Association, Capsid-binding Avidity and Retrovirus Restriction.** *J Virol* 2009, **83**:10737-51.
29. Mische CC, Javanbakht H, Song B, Diaz-Griffero F, Stremlau M, Strack B, Si Z, Sodroski J: **Retroviral restriction factor TRIM5alpha is a trimer.** *J Virol* 2005, **79**:14446-14450.
30. Javanbakht H, Yuan W, Yeung DF, Song B, Diaz-Griffero F, Li Y, Li X, Stremlau M, Sodroski J: **Characterization of TRIM5alpha trimerization and its contribution to human immunodeficiency virus capsid binding.** *Virology* 2006, **353**:234-246.
31. Nakayama EE, Maegawa H, Shioda T: **A dominant-negative effect of cynomolgus monkey tripartite motif protein TRIM5alpha on anti-simian immunodeficiency virus SIVmac activity of an African green monkey orthologue.** *Virology* 2006, **350**:158-163.
32. Perez-Caballero D, Hatziioannou T, Yang A, Cowan S, Bieniasz PD: **Human tripartite motif 5alpha domains responsible for retrovirus restriction activity and specificity.** *J Virol* 2005, **79**:8969-8978.
33. Sawyer SL, Wu LI, Emerman M, Malik HS: **Positive selection of primate TRIM5alpha identifies a critical species-specific retroviral restriction domain.** *Proc Natl Acad Sci USA* 2005, **102**:2832-2837.
34. Kono K, Song H, Shingai Y, Shioda T, Nakayama EE: **Comparison of anti-viral activity of rhesus monkey and cynomolgus monkey TRIM5alphas against human immunodeficiency virus type 2 infection.** *Virology* 2008, **373**:447-456.
35. Ohkura S, Yap MW, Sheldon T, Stoye JP: **All three variable regions of the TRIM5alpha B30.2 domain can contribute to the specificity of retrovirus restriction.** *J Virol* 2006, **80**:8554-8565.
36. Kono K, Bozek K, Domingues FS, Shioda T, Nakayama EE: **Impact of a single amino acid in the variable region 2 of the Old World monkey TRIM5alpha SPRY (B30.2) domain on anti-human immunodeficiency virus type 2 activity.** *Virology* 2009, **388**:160-168.
37. Perron MJ, Stremlau M, Sodroski J: **Two surface-exposed elements of the B30.2/SPRY domain as potency determinants of N-tropic murine leukemia virus restriction by human TRIM5alpha.** *J Virol* 2006, **80**:5631-5636.
38. Yap MW, Nisole S, Stoye JP: **A single amino acid change in the SPRY domain of human Trim5alpha leads to HIV-1 restriction.** *Curr Biol* 2005, **15**:73-78.
39. Stremlau M, Perron M, Welikala S, Sodroski J: **Species-specific variation in the B30.2(SPRY) domain of TRIM5alpha determines the potency of human immunodeficiency virus restriction.** *J Virol* 2005, **79**:3139-3145.
40. Sebastian S, Luban J: **TRIM5alpha selectively binds a restriction-sensitive retroviral capsid.** *Retrovirology* 2005, **2**:40.
41. Stremlau M, Perron M, Lee M, Li Y, Song B, Javanbakht H, Diaz-Griffero F, Anderson DJ, Sundquist WI, Sodroski J: **Specific recognition and accelerated uncoating of retroviral capsids by the TRIM5alpha restriction factor.** *Proc Natl Acad Sci USA* 2006, **103**:5514-5519.
42. Ylinen LM, Keckesova Z, Wilson SJ, Ranasinghe S, Towers GJ: **Differential restriction of human immunodeficiency virus type 2 and simian immunodeficiency virus SIVmac by TRIM5alpha alleles.** *J Virol* 2005, **79**:11580-11587.
43. Shibata R, Miura T, Hayami M, Ogawa K, Sakai H, Kiyomasu T, Ishimoto A, Adachi A: **Mutational analysis of the human immunodeficiency virus type 2 (HIV-2) genome in relation to HIV-1 and simian immunodeficiency virus SIV (AGM).** *J Virol* 1990, **64**:742-747.
44. Song H, Nakayama EE, Yokoyama M, Sato H, Levy JA, Shioda T: **A single amino acid of the human immunodeficiency virus type 2 capsid affects its replication in the presence of cynomolgus monkey and human TRIM5alphas.** *J Virol* 2007, **81**:7280-7285.
45. Ho SN, Hunt HD, Horton RM, Pullen JK, Pease LR: **Site-directed mutagenesis by overlap extension using the polymerase chain reaction.** *Gene* 1989, **77**:51-59.
46. Gyuris A, Vajda G, Foldes I: **Establishment of an MT4 cell line persistently producing infective HIV-1 particles.** *Acta Microbiol Hung* 1992, **39**:271-279.
47. Kuroishi A, Saito A, Shingai Y, Shioda T, Nomaguchi M, Adachi A, Akari H, Nakayama EE: **Modification of a loop sequence between alpha-helices 6 and 7 of virus capsid (CA) protein in a human immunodeficiency virus type 1 (HIV-1) derivative that has simian immunodeficiency virus (SIVmac239) vif and CA alpha-helices 4 and 5 loop improves replication in cynomolgus monkey cells.** *Retrovirology* 2009, **6**:70.
48. Price AJ, Marzetta F, Lammers M, Ylinen LM, Schaller T, Wilson SJ, Towers GJ, James LC: **Active site remodeling switches HIV specificity of antiretroviral TRIMCyp.** *Nat Struct Mol Biol* 2009, **16**:1036-1042.
49. Gamble TR, Yoo S, Vajdos FF, von Schwedler UK, Worthylake DK, Wang H, McCutcheon JP, Sundquist WI, Hill CP: **Structure of the carboxyl-terminal dimerization domain of the HIV-1 capsid protein.** *Science* 1997, **278**:849-853.
50. Pornillos O, Ganser-Pornillos BK, Kelly BN, Hua Y, Whitby FG, Stout CD, Sundquist WI, Hill CP, Yeager M: **X-ray structures of the hexameric building block of the HIV capsid.** *Cell* 2009, **137**:1282-1292.
51. Deshpande N, Addess KJ, Bluhm WF, Merino-Ott JC, Townsend-Merino W, Zhang Q, Knezevich C, Xie L, Chen L, Feng Z, Green RK, Flippen-Anderson JL, Westbrook J, Berman HM, Bourne PE: **The RCSB Protein Data Bank: a redesigned query system and relational database based on the mmCIF schema.** *Nucleic Acids Res* 2005, **33**:D233-237.
52. Shirakawa K, Takaori-Kondo A, Yokoyama M, Izumi T, Matsui M, Io K, Sato T, Sato H, Uchiyama T: **Phosphorylation of APOBEC3G by protein kinase A regulates its interaction with HIV-1 Vif.** *Nat Struct Mol Biol* 2008, **15**:1184-1191.
53. Labute P: **The generalized Born/volume integral implicit solvent model: estimation of the free energy of hydration using London dispersion instead of atomic surface area.** *J Comput Chem* 2008, **29**:1693-1698.
54. Ponder JW, Case DA: **Force fields for protein simulations.** *Adv Protein Chem* 2003, **66**:27-85.
55. Onufriev A, Bashford D, Case DA: **Modification of the generalized Born model suitable for macromolecules.** *Journal of Physical Chemistry B* 2000, **104**:3712-3720.
56. Onyangoa C, Leligdowicz A, Yokoyamac M, Sato H, Song H, Nakayama EE, Shioda T, Silva T, Townenda J, Jayea A, Whittle H, Rowland-Jones S, Cotten M: **HIV-2 capsids distinguish high and low virus load patients in a West African community cohort.** *Vaccine* 2010, **28S2**:60-67.
57. Braaten D, Franke EK, Luban J: **Cyclophilin A is required for the replication of group M human immunodeficiency virus type 1 (HIV-1) and simian immunodeficiency virus SIV(CPZ)GAB but not group O HIV-1 or other primate immunodeficiency viruses.** *J Virol* 1996, **70**:4220-4227.
58. Besnier C, Takeuchi Y, Towers G: **Restriction of lentivirus in monkeys.** *Proc Natl Acad Sci USA* 2002, **99**:11920-11925.
59. Cowan S, Hatziioannou T, Cunningham T, Muesing MA, Gottlinger HG, Bieniasz PD: **Cellular inhibitors with Fv1-like activity restrict human and simian immunodeficiency virus tropism.** *Proc Natl Acad Sci USA* 2002, **99**:11914-11919.
60. Hatziioannou T, Cowan S, Goff SP, Bieniasz PD, Towers GJ: **Restriction of multiple divergent retroviruses by Lv1 and Ref1.** *EMBO J* 2003, **22**:385-394.
61. Kootstra NA, Munk C, Tonnu N, Landau NR, Verma IM: **Abrogation of postentry restriction of HIV-1-based lentiviral vector transduction in simian cells.** *Proc Natl Acad Sci USA* 2003, **100**:1298-1303.
62. Owens CM, Song B, Perron MJ, Yang PC, Stremlau M, Sodroski J: **Binding and susceptibility to postentry restriction factors in monkey cells are specified by distinct regions of the human immunodeficiency virus type 1 capsid.** *J Virol* 2004, **78**:5423-5437.
63. Lin TY, Emerman M: **Determinants of cyclophilin A-dependent TRIM5 alpha restriction against HIV-1.** *Virology* 2008, **379**:335-341.
64. Hatziioannou T, Princiotta M, Piatak M Jr, Yuan F, Zhang F, Lifson JD, Bieniasz PD: **Generation of simian-tropic HIV-1 by restriction factor evasion.** *Science* 2006, **314**:95.

65. Berthoux L, Sebastian S, Sokolskaja E, Luban J: **Cyclophilin A is required for TRIM5{alpha}-mediated resistance to HIV-1 in Old World monkey cells.** *Proc Natl Acad Sci USA* 2005, **102**:14849-14853.
66. Keckesova Z, Ylinen LM, Towers GJ: **Cyclophilin A renders human immunodeficiency virus type 1 sensitive to Old World monkey but not human TRIM5 alpha antiviral activity.** *J Virol* 2006, **80**:4683-4690.
67. Sokolskaja E, Berthoux L, Luban J: **Cyclophilin A and TRIM5alpha independently regulate human immunodeficiency virus type 1 infectivity in human cells.** *J Virol* 2006, **80**:2855-2862.
68. Stremlau M, Song B, Javanbakht H, Perron M, Sodroski J: **Cyclophilin A: an auxiliary but not necessary cofactor for TRIM5alpha restriction of HIV-1.** *Virology* 2006, **351**:112-120.
69. Khorasanizadeh S, Campos-Olivas R, Clark CA, Summers MF: **Sequence-specific 1H, 13C and 15N chemical shift assignment and secondary structure of the HTLV-I capsid protein.** *Journal of biomolecular NMR* 1999, **14**:199-200.
70. Jin Z, Jin L, Peterson DL, Lawson CL: **Model for lentivirus capsid core assembly based on crystal dimers of EIAV p26.** *J Mol Biol* 1999, **286**:83-93.
71. Mortuza GB, Dodding MP, Goldstone DC, Haire LF, Stoye JP, Taylor IA: **Structure of B-MLV capsid amino-terminal domain reveals key features of viral tropism, gag assembly and core formation.** *J Mol Biol* 2008, **376**:1493-1508.
72. Mortuza GB, Goldstone DC, Pashley C, Haire LF, Palmarini M, Taylor WR, Stoye JP, Taylor IA: **Structure of the capsid amino-terminal domain from the betaretrovirus, Jaagsiekte sheep retrovirus.** *J Mol Biol* 2009, **386**:1179-1192.
73. Kinomoto M, Appiah-Opong R, Brandful JA, Yokoyama M, Nii-Trebi N, Ugly-Kwame E, Sato H, Ofori-Adjei D, Kurata T, Barre-Sinoussi F, Sata T, Tokunaga K: **HIV-1 proteases from drug-naive West African patients are differentially less susceptible to protease inhibitors.** *Clin Infect Dis* 2005, **41**:243-251.
74. Kinomoto M, Yokoyama M, Sato H, Kojima A, Kurata T, Ikuta K, Sata T, Tokunaga K: **Amino acid 36 in the human immunodeficiency virus type 1 gp41 ectodomain controls fusogenic activity: implications for the molecular mechanism of viral escape from a fusion inhibitor.** *J Virol* 2005, **79**:5996-6004.

doi:10.1186/1742-4690-7-72
Cite this article as: Kono *et al.*: Multiple sites in the N-terminal half of simian immunodeficiency virus capsid protein contribute to evasion from rhesus monkey TRIM5α-mediated restriction. *Retrovirology* 2010 7:72.